Open
ORIGINAL ARTICLE

Cell Research (2014) 24:680-700.

www.nature.com/cr

Pachytene piRNAs instruct massive mRNA elimination during late spermiogenesis

Lan-Tao Gou[1, 2, *], Peng Dai[1, 2, *], Jian-Hua Yang[3, *], Yuanchao Xue[4], Yun-Ping Hu[1, 2], Yu Zhou[4], Jun-Yan Kang[1, 2], Xin Wang[1, 2], Hairi Li[4], Min-Min Hua[1, 2], Shuang Zhao[1, 2], Si-Da Hu[1, 2], Li-Gang Wu[1, 2], Hui-Juan Shi[5], Yong Li[6], Xiang-Dong Fu[4], Liang-Hu Qu[3], En-Duo Wang[1], Mo-Fang Liu[1, 2]

[1]Center for RNA Research, State Key Laboratory of Molecular Biology–University of Chinese Academy of Sciences, Shanghai 200031, China; [2]Shanghai Key Laboratory of Molecular Andrology, Institute of Biochemistry and Cell Biology, Shanghai Institutes for Biological Sciences, Chinese Academy of Sciences, Shanghai 200031, China; [3]Key Laboratory of Gene Engineering of the Ministry of Education, State Key Laboratory of Biocontrol, Sun Yat-sen University, Guangzhou, Guangdong 510275, China; [4]Department of Cellular and Molecular Medicine, University of California, San Diego, La Jolla, CA 92093-0651, USA; [5]National Population and Family Planning Committee Key Laboratory of Contraceptive Drugs & Devices, Shanghai Institute of Planned Parenthood Research, Shanghai 200032, China; [6]Department of Biochemistry and Molecular Biology and Center for Genetics and Molecular Medicine, School of Medicine, University of Louisville, Louisville, KY 40202, US

Spermatogenesis in mammals is characterized by two waves of piRNA expression: one corresponds to classic piRNAs responsible for silencing retrotransponsons and the second wave is predominantly derived from nontransposon intergenic regions in pachytene spermatocytes, but the function of these pachytene piRNAs is largely unknown. Here, we report the involvement of pachytene piRNAs in instructing massive mRNA elimination in mouse elongating spermatids (ES). We demonstrate that a piRNA-induced silencing complex (pi-RISC) containing murine PIWI (MIWI) and deadenylase CAF1 is selectively assembled in ES, which is responsible for inducing mRNA deadenylation and decay via a mechanism that resembles the action of miRNAs in somatic cells. Such a highly orchestrated program appears to take full advantage of the enormous repertoire of diversified targeting capacity of pachytene piRNAs derived from nontransposon intergenic regions. These findings suggest that pachytene piRNAs are responsible for inactivating vast cellular programs in preparation for sperm production from ES.

***Keywords*:** pachytene piRNAs; MIWI; CAF1; pi-RISC; mRNA deadenylation; ES
Cell Research (2014) **24**:680-700. doi:10.1038/cr.2014.41; published online 2 May 2014

Introduction

Piwi-interacting RNAs (piRNAs) represent a distinct class of germ cell-specific noncoding RNAs in animals [1-4]. This class of small RNAs is specifically associated with Piwi proteins, which are germline-specific members of the Argonaute protein family [5-9]. It has been well documented that Piwi proteins are required for both biogenesis and function of piRNAs [10-14]. Genetic studies in mouse, *Drosophila*, zebrafish, and *C. elegans* demonstrate a critical function of the piRNA pathway in silencing mobile genetic elements in animal germ cells [14-16]. However, it has been unclear whether prevention of unwanted spreading of mobile genetic elements is sufficient to account for the essential role of the piRNA system in gametogenesis.

The mouse genome contains three *Piwi* family members, *Mili*, *Miwi*, and *Miwi2*, which are temporally and spatially regulated during male germ cell differentiation and all proven to be essential for spermatogenesis [15]. In mice, piRNAs are expressed in two distinct phases during male germ cell development, respectively termed as pre-pachytene and pachytene piRNAs [17]. Pre-pachytene piRNAs, which are enriched in transposon sequenc-

*These three authors contributed equally to this work.
Correspondence: Mo-Fang Liu
Tel: 86 21 54921146; Fax: 86 21 54921011
E-mail: mfliu@sibcb.ac.cn
Received 17 January 2014; revised 26 February 2014; accepted 2 March 2014; published online 2 May 2014

es and coexpressed with MIWI2 and/or MILI in early stages of spermatogenesis, are primarily involved in *de novo* DNA methylation in fetal and perinatal male germ cells [11, 18, 19]. The function of pachytene piRNAs, which are massively induced mainly from nontransposon intergenic regions in pachytene spermatocytes and post-meiotic spermatids, has been largely unknown.

In addition, development of post-meiotic male germ cells in animals is known as a complex biochemical and morphological process, consisting of at least 16 sequential transition steps in mice [20]. The dramatic differentiation process called spermiogenesis includes acrosome and flagellum formation, nuclear condensation, and cytoplasmic exclusion [21]. Through these sequential programmed transitions, haploid spermatids are eventually transformed into sperms. Interestingly, from the point of view of selective maternal or paternal contributions to early life events, oocytes contain abundant proteins and mRNAs whereas sperms retain little mRNAs and their genetic information is only expressed after zygotic activation [22, 23]. How mRNAs in spermatids are massively eliminated during late spermiogenesis has remained largely unexplored.

In this study, we document an unexpected finding that pachytene piRNAs are responsible for eliminating bulk mRNAs in spermatids during spermiogenesis. In this process, pachytene piRNAs are assembled with MIWI and deadenylase CAF1 to form a piRNA-induced silencing complex (pi-RISC), which promotes deadenylation and decay of their target mRNAs. CAF1, a key catalytic subunit of the CCR4-CAF1-NOT deadenylase complex [24], is abundantly expressed in mouse testes and is known to be essential to spermatogenesis [25]. Inhibition of the pi-RISC function by knocking down either *Miwi* or *Caf1* or blocking piRNA action elevated the levels of specific piRNA target mRNAs in elongating spermatids (ES). Strikingly, > 7 300 out of ~12 000 mRNAs detectable in ES were physically associated with MIWI, while ~5 000 protein genes in ES were significantly upregulated upon *Miwi* or *Caf1* knockdown, of which ~90% were commonly regulated by MIWI and CAF1. Moreover, the majority of mRNAs could each be matched with a specific set of piRNAs and the levels of mRNAs were inversely correlated with the numbers of potential piRNA target sites as well as the abundance of matched piRNAs expressed in ES. These results reveal a male germ cell-specific mRNA degradation program that utilizes the enormous repertoire of diversified targeting capacity of pachytene piRNAs. The newly elucidated function of pachytene piRNAs coupled with the established role of pre-pachytene piRNAs in silencing transposons further emphasizes a vital functional requirement for the piRNA system in male germ cell development in mammals.

Results

The MIWI complex in ES harbors both piRNAs and mRNAs

mRNAs are abundantly expressed in post-meiotic spermatids but much fewer remain in sperms [23, 26, 27], suggesting that a large variety of mRNAs in spermatids are massively eliminated in late stages of spermatid development; however, the mechanism responsible for such a highly synchronized program has remained elusive. Considering the coincident expression of piRNAs and their ability to induce degradation of transposon-derived transcripts in male germ cells [14, 15], we hypothesize that pachytene piRNAs might be instrumental to this key developmental process in spermiogenesis. To test this hypothesis, we isolated MIWI/RNA complexes from enriched mouse ES by RNA immunoprecipitation (RIP) with an anti-MIWI antibody (Figure 1A). On polyacrylamide gel, we noticed the presence of abundant small RNAs as well as a population of large RNAs in isolated MIWI complexes (Figure 1B).

To characterize the MIWI-associated RNAs, we first performed deep sequencing on the small RNAs ranging from 19 to 40 nt in length, and identified 715 144 unique reads (from a total of 27 644 384 reads, of which 25 697 817 could be mapped to the mouse genome) present in the MIWI immunoprecipitates, but not the IgG control processed in parallel (Supplementary information, Table S1). As expected, the majority of the small RNA reads corresponds to candidate piRNAs of 29-31 nt in length with the typical uracil residue (U) at their 5'-termini (Supplementary information, Figure S1A). In addition to such length characteristics, these small RNAs appear to depend on MIWI for their functions in male germ cells, thus further qualifying them as piRNAs (see below). Interestingly, we found that these MIWI-associated piRNAs are largely derived from nontransposon intergenic regions, which has been similarly observed in other laboratories [28, 29]. This observation suggests that the piRNA machinery may have additional function(s) beyond transposon silencing.

We next performed deep sequencing on the large RNAs (> 200 nt) associated with the MIWI complex, and obtained a total of 1 499 244 unique reads (from a total of 19 174 539 reads) (Supplementary information, Table S1). While ~67% of these large RNAs match transposon-derived transcripts, a significant fraction (> 20%) of them corresponds to protein-coding mRNAs expressed in ES. Therefore, the MIWI complex in ES appears to harbor both nontransposon-derived piRNAs and specific mRNAs.

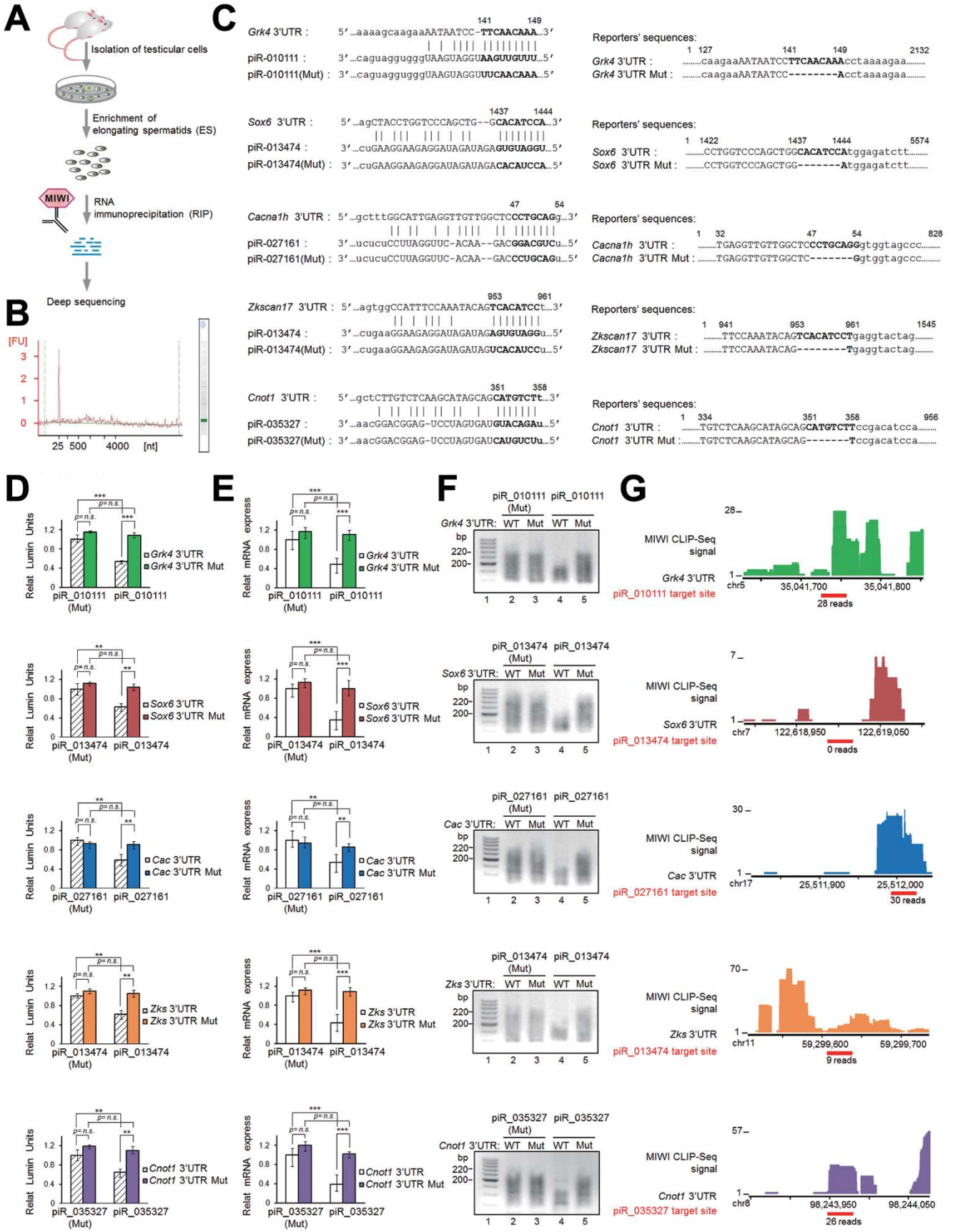
A
Isolation of testicular cells
Enrichment of elongating spermatids (ES)
MIWI
RNA immunoprecipitation (RIP)
Deep sequencing
B
[FU]
3
2
1
0
25 500
4000
[nt]
C
Grk4 3'UTR : 5′…aaaagcaagaaAATAATCC-TTCAACAAA…3′
piR-010111 : 3′…caguaggugggUAAGUAGGUAAGUUGUUU…5′
piR-010111(Mut) : 3′…caguaggugggUAAGUAGGUUUCAACAAA…5′
Reporters' sequences:
Grk4 3'UTR : ……caagaaAATAATCCTTCAACAAAcctaaaagaa……
Grk4 3'UTR Mut : ……caagaaAATAATCC--------Acctaaaagaa……
Sox6 3'UTR : 5′…agCTACCTGGTCCCAGCTG--GCACATCCA…3′
piR-013474 : 3′…cuGAAGGAAGAGGAUAGAUAGAGUGUAGGU…5′
piR-013474(Mut) : 3′…cuGAAGGAAGAGGAUAGAUAGACACAUCCA…5′
Reporters' sequences:
Sox6 3'UTR : ……CCTGGTCCCAGCTGGCACATCCAtggagatctt……
Sox6 3'UTR Mut : ……CCTGGTCCCAGCTGG-------Atggagatctt……
Cacna1h 3'UTR : 5′…gctttGGCATTGAGGTTGTTGGCTCCCTGCAGg…3′
piR-027161 : 3′…ucucuCCUUAGGUUC-ACAA--GACGGACGUCu…5′
piR-027161(Mut) : 3′…ucucuCCUUAGGUUC-ACAA--GACCCUGCAGu…5′
Reporters' sequences:
Cacna1h 3'UTR : ……TGAGGTTGTTGGCTCCCTGCAGGgtggtagccc……
Cacna1h 3'UTR Mut : ……TGAGGTTGTTGGCTC-------Ggtggtagccc……
Zkscan17 3'UTR : 5′…agtggCCATTTCCAAATACAGTCACATCCt…3′
piR-013474 : 3′…cugaaGGAAGAGGAUAGAUAGAGUGUAGGu…5′
piR-013474(Mut) : 3′…cugaaGGAAGAGGAUAGAUAGUCACAUCCu…5′
Reporters' sequences:
Zkscan17 3'UTR : ……TTCCAAATACAGTCACATCCTgaggtactag……
Zkscan17 3'UTR Mut : ……TTCCAAATACAG--------Tgaggtactag……
Cnot1 3'UTR : 5′…gctCTTGTCTCAAGCATAGCAGCATGTCTt…3′
piR-035327 : 3′…aacGGACGGAG-UCCUAGUGAUGUACAGAu…5′
piR-035327(Mut) : 3′…aacGGACGGAG-UCCUAGUGAUCAUGUCUu…5′
Reporters' sequences:
Cnot1 3'UTR : ……TGTCTCAAGCATAGCAGCATGTCTTccgacatcca……
Cnot1 3'UTR Mut : ……TGTCTCAAGCATAGCAG-------Tccgacatcca……
D
Relat Lumin Units
p=n.s.
***
**
Grk4 3'UTR
Grk4 3'UTR Mut
Sox6 3'UTR
Sox6 3'UTR Mut
Cac 3'UTR
Cac 3'UTR Mut
Zks 3'UTR
Zks 3'UTR Mut
Cnot1 3'UTR
Cnot1 3'UTR Mut
piR_010111 piR_010111 (Mut)
piR_013474 piR_013474 (Mut)
piR_027161 piR_027161 (Mut)
piR_035327 piR_035327 (Mut)
E
Relat mRNA express
F
piR_010111 piR_010111 (Mut)
piR_013474 piR_013474 (Mut)
piR_027161 piR_027161 (Mut)
piR_035327 piR_035327 (Mut)
Grk4 3'UTR: WT Mut WT Mut
Sox6 3'UTR: WT Mut WT Mut
Cac 3'UTR: WT Mut WT Mut
Zks 3'UTR: WT Mut WT Mut
Cnot1 3'UTR: WT Mut WT Mut
bp
220-
200-
1 2 3 4 5
G
MIWI CLIP-Seq signal
Grk4 3'UTR
piR_010111 target site
chr5
35,041,700
35,041,800
28 reads
Sox6 3'UTR
piR_013474 target site
chr7
122,618,950
122,619,050
0 reads
Cac 3'UTR
piR_027161 target site
chr17
25,511,900
25,512,000
30 reads
Zks 3'UTR
piR_013474 target site
chr11
59,299,600
59,299,700
9 reads
Cnot1 3'UTR
piR_035327 target site
chr8
98,243,950
98,244,050
26 reads

Figure 1 piRNAs act like miRNAs to induce mRNA deadenylation and decay. **(A)** Strategy to identify RNAs associated with MIWI in ES by RIP. **(B)** Urea-polyacrylamide gel electrophoresis analyses of MIWI RIPed-RNAs. Left, densities of RNAs at size range of measurement. Right, representative image of urea-polyacrylamide gel. **(C)** Predicted piRNA regulatory elements at the 3′UTRs of *Grk4*, *Sox6*, *Cacna1h*, *Zkscan17*, and *Cnot1*, and the sequences of synthetic piRNAs, negative control piRNA(Mut), and wild-type 3'UTR and mutated 3′UTR Mut-*Renilla* luciferase reporters. **(D)** Dual-luciferase reporter assays of the effect of piRNAs on reporter activities in GC-2spd(ts) cells, with cognate piRNA(Mut) serving as negative controls. **(E)** qRT-PCR analyses of the effect of piRNAs on reporter mRNA levels. **(F)** PAT assays of the effect of piRNAs on reporter Poly(A) tails. **(G)** Verification of piRNA target sites by MIWI CLIP. Top, the cluster of MIWI CLIP tags on the five validated piRNA target genes (one color per gene). The scales in genes were numbered following the dimension of their respective chromosomes. Bottom, the red thick lines indicated piRNA target sites. The indicated numbers at top left represent the highest reads of CLIP tags for cognate genes, and those under red thick lines show the reads of CLIP tags that perfectly matched to cognate target sites. The average values ± S.D. of three separate experiments were plotted. $^{**}P < 0.01$, $^{***}P < 0.001$. Results shown are representative of three independent experiments.

piRNAs repress target mRNAs via the imperfectly base-pairing rule

To determine the potential relationship between piRNAs and mRNAs in the MIWI complexes, we asked how the piRNAs might be related to the mRNAs in sequences. Using the miRanda program [30], we searched potential targeting sites of MIWI-associated piRNAs within the 3′UTRs of MIWI-associated mRNAs. Focusing on abundant piRNAs (reads ≥ 1 000), for example, we noted that nearly all highly enriched mRNAs in the MIWI complexes could be each matched to a specific set of piRNAs. This resulted in a predicted set of 45 075 piRNA:mRNA interactions that involve 2 861 piRNAs identified in the MIWI complex (the top five scored pairs listed in Supplementary information, Table S2), with each piRNA having the potential to target ~16 mRNAs on average (Supplementary information, Figure S1B). These findings raise an intriguing possibility that the MIWI-associated piRNAs might regulate their target mRNAs via a miRNA-like mechanism in ES.

We next performed the reporter-based assay to evaluate the functional consequence of the predicted piRNA:mRNA interactions. We selected a set of 10 piRNA:mRNA pairs (all with the miRanda alignment score > 150 and the selected piRNA with reads > 10 000, see Table 1), and in each case, both wild-type and mutant (containing deletion of the 7-8 bp region complementary to the 5′ portion of corresponding piRNA) 3′UTRs of the predicted targets were placed downstream of the *Renilla* luciferase reporter (Figure 1C). A mouse spermatocyte cell line GC-2spd(ts) [31], in which we found that most key components of the piRNA pathway (i.e., piRNAs, MIWI, MILI and etc.) as well as MIWI/piRNA complexes were present (Supplementary information, Figure S2A-S2D), was used as an *in vitro* model system for probing the potential molecular mechanisms of piRNAs.

When the reporters were cotransfected along with cognate chemically synthesized piRNAs (containing phosphate at the 5′ end and 2′-O-methylation at the 3′ end) into GC-2spd(ts) cells, we found that 5 out of the 10 tested reporters, but not their mutant versions, were significantly repressed by cotransfected piRNAs (i.e., *Grk4* by piR_010111, *Sox6* and *Zkscan17* by piR_013474, *Cacna1h* by piR_027161, and *Cnot1* by piR_035327; see Figure 1D). RT-qPCR analysis of individual reporter mRNAs revealed similar piRNA-targeting dependent responses, indicating that piRNAs induce mRNA degradation (Figure 1E). Furthermore, we found that *Grk4* was expressed in GC-2spd(ts) cells, and transfection of piR_010111 significantly reduced endogenous *Grk4* mRNA level (Supplementary information, Figure S2E). Interestingly, *Miwi* knockdown marginally affected *Grk4* mRNA level in GC-2spd(ts) cells likely due to the lack of endogenous piR_010111 in these cells, but dramatically attenuated the effect of piR_010111 on *Grk4* expression in piR_010111-transfected cells (Supplementary information, Figure S2F). Although the other five candidate targets (i.e., *Nploc4*, *Samd4*, *Qrich1*, *Tcf20*, and *Ap2a1*) were nonresponsive to the selected piRNAs in our reporter assays, it remains possible that they might be targeted by other piRNAs because each contains potential binding sites for multiple other piRNAs; this was proven to be the case after we pinpointed specific MIWI-binding sites in these mRNAs by using crosslinking immunoprecipitation coupled with deep sequencing (CLIP-seq) (see below).

To further characterize the piRNA-mediated mRNA decay, we determined whether deadenylation, which is a well-known mechanism underlying miRNA-mediated mRNA decay [32], is involved in this piRNA-induced mRNA decay. By performing the poly(A) test (PAT) assay, we found that each cotransfected piRNA was able to specifically induce shortening of the poly(A) tail of the corresponding wild-type reporter, but not the mutant form (Figure 1F). Together, these results reveal that piRNAs induce mRNA deadenylation and decay through im-

Table 1 The selected piRNA:mRNA pairs for reporter-based validation

piRNA	Predicted target of piRNA	Predicted piRNA:mRNA interaction
piR_010111	*Grk4**	piRNA:3'-agtaggtgggTAAGTAGGTAAGTTGTTt-5' mRNA: 5'-aaagcaagaaAATAATCC-TTCAACAAa-3'
piR_013474	*Sox6**	piRNA 3'-ctGAAGGAAGAGGATAGATAGAGTGTAGGt-5' mRNA 5'-agCTACCTGGTCCCAGCTG--GCACATCCa-3'
piR_027161	*Cacna1h**	piRNA 3'-tctctCCTTAGGTTC-ACAA--GACGGACGTCt-5' mRNA 5'-gctttGGCATTGAGGTTGTTGGCTCCCTGCAGg-3'
piR_013474	*Zkscan17**	piRNA:3'-ctgaaGGAAGAGGATAGATAGAGTGTAGGt-5' mRNA: 5'-agtggCCATTTCCAAATACAGTCACATCCt-3'
piR_035327	*Cnot1**	piRNA 3'-aacGGACGGAG-TCCTAGTGATGTACAGAt-5' mRNA 5'-gctCTTGTCTCAAGCATAGCAGCATGTCTt-3'
piR_037194	*Nploc4*	piRNA 3'-tgAAGGGGA-TCGTTGGGAACTTTGGAGTCt-5' mRNA 5'-atTTCTCCTCAGAAGC-----AAACCTCAGt-3'
piR_000320	*Samd4*	piRNA 3'-ccACCTATCACGGTTAGTAGGATGTTACGTa-5' mRNA 5'-ttTGCCTAGTTCATGTTGCCAAGCAATGCAt-3'
piR_007526	*Qrich1*	piRNA 3'-cgggtggTTAGATAGTAGTAGGTGAACAt-5' mRNA 5'-tgatggaATTCTTGTAACATACACTTGTg-3'
piR_028076	*Tcf20*	piRNA 3'-tcgGTATTAAGGTACTCAAAAAGAAAGGTt-5' mRNA 5'-aaaCACAAATAAAT--TTTTTTCTTTCCAg-3'
piR_031456	*Ap2a1*	piRNA 3'-ccACTAAGACTGATGAAGGTGACGACAAt-5' mRNA 5'-ttTTATTTTTGTT-CATCTGCTGCTGTTt-3'

* indicated the reporter significantly repressed by the selected piRNA.

perfectly base-pairing with specific sites in the 3′UTRs of target transcripts.

Verification of piRNA target sites by MIWI CLIP-seq

The above results show that specific piRNA target sites are required for piRNA-mediated target repression (Figure 1D-1F), which prompted us to ask whether MIWI physically associates with piRNA target sites. To this end, we performed MIWI CLIP-seq on isolated ES (Supplementary information, Figure S3A), which identified 23 928 416 unique reads that are mapped to the mouse genome, and gave rise to a total of 186 157 piRNAs and 7 382 mRNAs at a cut-off of five reads (Supplementary information, Figure S3B and Table S3). This confirms our earlier observation that MIWI is broadly associated with both piRNAs and mRNAs (Figure 1B and Supplementary information, Table S1). Again, the piRNAs and mRNAs in MIWI complexes are significantly related in sequences as shown by analyses using the miRanda software [30] (Supplementary information, Figure S3C), further supporting that piRNAs regulate their target mRNAs via a base-pairing rule in ES. Interestingly, MIWI tags were distributed at all regions in mRNAs with some enrichment near the stop codon and the poly(A) site (Supplementary information, Figure S3D), a pattern similar to Ago2-RNA interactions. However, the enrichment at the 3′UTRs is greatly reduced compared to the Ago2 RNA map as we recently reported

[33], suggesting a much less effect from the scanning ribosome. Consistent with our observation, recent studies in *C. elegans* suggest that piRNAs utilize imperfect base-pairing to scan germline-expressed mRNAs [34, 35]. Noticeably, the CLIP-seq data also revealed the association of MIWI with other types of RNAs, including a large number of long noncoding RNAs (Supplementary information, Table S3), which will be separately pursued.

Importantly, the CLIP-seq data provide reliable information on actual MIWI action sites. Indeed, all of the 10 previously selected candidate piRNA targets (see Table 1) contained specific MIWI-binding sites (Figure 1G and Supplementary information, Figure S3E). Specific MIWI-CLIP tags were clearly centered in four out of the five predicated piRNA-binding sites (in *Grk4* by piR_010111, *Zkscan17* by piR_013474, *Cacna1h* by piR_027161, and *Cnot1* by piR_035327) (Figure 1G). Nevertheless, we note that the sequence reads of *Sox6* (peaked at ~30 nt downstream of the target site by piR_013474) were much less than those of others, likely due to a low expression of this gene in ES. Utilizing the mapped MIWI binding peaks as guide, we searched for additional potential piRNA target sites on the other five candidate targets that were previously shown to be nonresponsive to the "predicted" piRNAs (Supplementary information, Figure S3E). This led to five newly predicted piRNA:mRNA pairs (i.e., piR_005092:*Nploc4*, piR_12800:*Samd4*, piR_007526:*Qrich1*, piR_009524:*Tcf20,* and piR_018939:*Ap2a1* in Supplementary information, Figure S3F, left) and importantly, all of these five newly predicted piRNA:mRNA interactions could be experimentally verified with the reporter-based assays (Supplementary information, Figure S3F, right). Taken together, these results indicate that MIWI CILP-seq is effective in identifying piRNA targets and pinpointing specific piRNA action sites in the targets.

MIWI is required for piRNA-mediated mRNA decay

An important criterion for classifying MIWI-associated small RNAs as piRNAs is whether they depend on MIWI to function *in vivo*. To test this functional requirement, we asked whether MIWI, which is endogenously expressed in GC-2spd(ts) cells (Supplementary information, Figure S2B), is required for target repression in response to cognate piRNAs. We examined the effect of *Miwi* knockdown on the piRNA-responsive reporters, and found that the *Miwi* siRNA (*Miwi* siR), but not a scrambled control siRNA (Scr siR), dramatically attenuated the effect of piR_010111 on the *Grk4* reporter activity and deadenylation of the reporter mRNA in transfected GC-2spd(ts) cells (Figure 2A). We obtained similar results with all other four reporters we examined, including the *Sox6* reporter targeted by piR_013474, the *Cacna1h* reporter by piR_027161, the *Zkscan17* reporter by piR_013474, and the *Cnot1* reporter by piR_035327 (Supplementary information, Figure S4A). To determine whether MIWI promotes the turnover of candidate piRNA targets in GC-2spd(ts) cells, we used miRanda [30] to search for potential targets of piR_005901, a piRNA expressed in both GC-2spd(ts) cells and ES, in the 3'UTR of MIWI-CLIPed mRNAs. We selected top four candidate piR_005901 targets including *Msrb3*, *Ddt*, *Dcaf8,* and *Mlec*, for further evaluation (Supplementary information, Figure S2G). We found that the mRNA levels of all these four genes were significantly upregulated upon MIWI knockdown in GC-2spd(ts) cells, while the expression of nontarget *GAPDH* was little affected (Supplementary information, Figure S2H and S2I).

Given that *Mili*, another *Piwi* member, is also expressed in GC-2spd(ts) cells (Supplementary information, Figure S2B), we also examined whether MILI plays a role in piRNA-mediated target repression. Interestingly, knockdown of *Mili* appeared to cause little change in piRNA-dependent reporter repression (Supplementary information, Figure S4B), indicating that MILI is dispensable for such regulation. In agreement, our RIP assays showed that, unlike MIWI, MILI pulled down much less amount of cotransfected 30 nt piRNAs (Supplementary information, Figure S4C), which is consistent with the established preference of MIWI for piRNAs peaked at ~30 nt and MILI for piRNAs at ~26 nt [1, 2]. Furthermore, considering the fact that Ago2, a key miRNA/siRNA-RISC component, is ubiquitously expressed in both somatic and germ cells, we knocked down *Ago2* in GC-2spd(ts) cells, and again, detected little, if any, impact on piRNA function (Supplementary information, Figure S4B). Similarly, we found that Ago2 was barely associated with transfected piRNAs but specifically with 19 nt Scr siR (Supplementary information, Figure S4C), which is fully consistent with the established rules for loading of different small RNAs into distinct Argonaute proteins [36]. These data strongly suggest that piRNAs do not utilize the miRNA/siRNA machinery for target repression, thus providing further evidence that the MIWI-associated small RNAs act as piRNAs and function in target repression in a strictly MIWI-dependent manner. We further strengthened this conclusion by overexpressing MIWI in GC-2spd(ts) cells, finding that ectopically expressed Flag-MIWI protein could further enhance the repression of the *Grk4* reporter by piR_010111 and other four reporters by their cognate piRNAs (Figure 2B and Supplementary information, Figure S4D).

We next wished to determine whether the slicer activity of MIWI is required for piRNA-mediated target

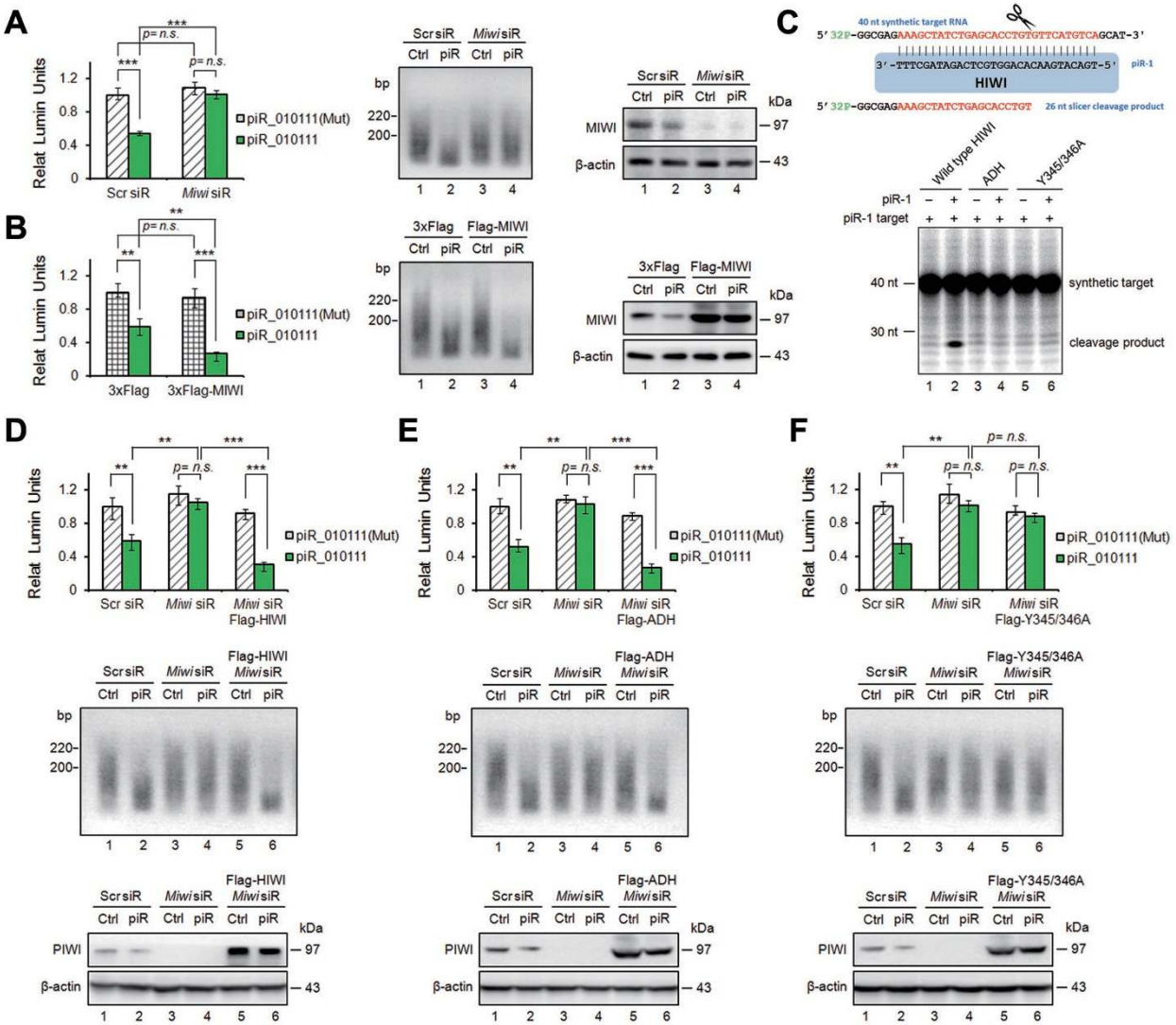

Figure 2 MIWI is required for piRNA-induced target repression. **(A** and **B)** The effect of *Miwi* knockdown **(A)** or ectopic Flag-MIWI **(B)** on piR_010111-induced *Grk4* reporter repression in GC-2spd(ts) cells. Left, dual-luciferase reporter assays. Middle, PAT assays. Right, western blot assays of MIWI proteins, with β-actin serving as a loading control. **(C)** *In vitro* slicer activity assays of wildtype HIWI (lanes 1 and 2), and its slicer activity-deficient ADH (lanes 3 and 4) and piRNA loading-deficient Y345/346A mutants (lanes 5 and 6). Left, Scheme showing the synthetic 40 nt RNA target for piR-1 as well as the expected cleavage products. Right, Slicer assay with HIWI complexes (purified with Flag antibody) and a 5′-[^{32}P]-labeled RNA target bearing complementarity to piR-1. Lanes 1, 3, and 5, HIWI or its mutants purified from the cells transfected with Flag-HIWI or its mutant expression vectors; lanes 2, 4, and 6, HIWI/piR-1 complexes purified from GC-2spd(ts) cells cotransfected with respective HIWI constructs and piR-1. **(D**-**F)** Ectopic Flag-HIWI **(D)** or Flag-ADH HIWI mutant **(E)**, but not Flag-Y345/346 HIWI mutant **(F)**, rescued piR_010111-induced *Grk4* reporter repression in *Miwi siR*-treated GC-2spd (ts) cells. Top, dual-luciferase reporter assays. Middle, PAT assays. Bottom, western blot assays of PIWI proteins, with β-actin serving as a loading control. The average values ± s.d. of three separate experiments were plotted. ***P* < 0.01, ****P* < 0.001. Results shown are representative of three independent experiments.

repression. To this end, we constructed a slicer activity-deficient ADH mutant [13] of human PIWI (HIWI) (Figure 2C), which is highly homologous (~94% identity) to MIWI [6], and cotransfected the construct with piR_010111 and the *Grk4* reporter into *Miwi* siR-treated GC-2spd(ts) cells. Western blot confirmed equivalent expression of both wild-type and mutant HIWI in *Miwi* siR-treated cells (Figure 2D-2F, bottom panels). Interestingly, both wild-type and ADH mutant HIWI were able to restore piR_010111-dependent repression of the

Grk4 reporter in MIWI-depleted GC-2spd(ts) cells (Figure 2D and 2E), suggesting that the function of MIWI in this context is independent of its slicer activity. By contrast, Flag-Y345/346A HIWI, a mutant defective in piRNA loading [37], failed to restore the piRNA function in *Miwi* siR-treated cells (Figure 2F). Northern blot confirmed that piRNA was able to significantly load onto wild-type and ADH mutant HIWI, but not Y345/346A mutant (Supplementary information, Figure S4E). These data demonstrate that the piRNA-loading ability, but not the slicer activity of MIWI, is required to execute piRNA-mediated target repression.

CAF1 functions as a specific partner of MIWI in piRNA-mediated mRNA decay

Having demonstrated the ability of piRNAs in inducing mRNA deadenylation and decay that depends on MIWI, but not its slicer activity, we reasoned that an additional cofactor(s), likely a deadenylase(s), might be involved in this process. Given that CAF1 is known to play a key role in miRNA-mediated mRNA deadenylation and decay in somatic cells [38], and that it is also highly expressed in mouse testes and shown to be required for male fertility [25], we tested its potential involvement in piRNA action in male germ cells. We first determined whether MIWI interacts with CAF1 by co-immunoprecipitation (co-IP), and found that Flag-MIWI and Myc-CAF1 indeed efficiently pulled down one another in cotransfected GC-2spd(ts) cells (Figure 3A) and their interaction was independent of piRNAs (Supplementary information, Figures S5A). In contrast, MILI showed little interaction with CAF1 under the same experimental conditions (Supplementary information, Figure S5B). We next performed *in vitro* GST pulldown assays and found that GST-CAF1, but not GST control, brought down *in vitro* translated [^{35}S]Met-MIWI, indicative of a direct interaction between the two proteins (Figure 3B). We further extended the analysis *in vivo*, demonstrating that endogenous CAF1 interacts with MIWI in adult mouse testes and their interaction is resistant to RNase A treatment (Figure 3C). Together, these results established a physical interaction between MIWI and CAF1.

We next examined whether CAF1 is essential for piRNA-induced target repression. Indeed, *Caf1* siRNA significantly attenuated the effect of piR_010111 on both the *Grk4* reporter activity and reporter mRNA deadenylation in GC-2spd(ts) cells (Figure 3D). This is also true with all other reporters (*Sox6*, *Cacna1h*, *Zkscan17,* and *Cnot1*) we tested (Supplementary information, Figure S5C). Conversely, ectopic expression of Myc-CAF1 strengthened the repression of individual reporters by their cognate piRNAs in transfected cells (Figure 3E and Supplementary information, Figure S5D). These results demonstrate that CAF1 is required for piRNA-mediated target repression.

Given that CAF1 is a major catalytic subunit of the CCR4-CAF1-NOT deadenylase complex [24], we next asked whether other subunit(s) of the deadenylase complex might be similarly required for piRNA-mediated mRNA deadenylation and decay. Interestingly, knockdown of *Cnot1*, which is essential for miRNA-induced gene silencing [39, 40], only marginally affected the effect of piR_010111 on the *Grk4* reporter activity (Supplementary information, Figure S5E, top). This finding suggests that piRNAs employ a distinct machinery from miRNAs in gene silencing. Intriguingly, we note that *Cnot1* itself is a target of piRNAs. Moreover, knockdown of *Cnot6* (*CCR4a*), which encodes another catalytic subunit of the CCR4-CAF1-NOT deadenylase complex [24], also only slightly impaired the effect of piR_010111 on the *Grk4* reporter (Supplementary information, Figure S5E, bottom). Together, these results imply that the classical miRNA machinery *per se* makes little contribution to piRNA-programmed mRNA elimination in male germ cells, which is fully in line with the observation that the CAF1 protein, but not CNOT1 and CNOT6, is dramatically increased in mouse testes (Supplementary information, Figure S5F).

To further establish the unique partnership of CAF1 with the MIWI/piRNA complex, we determined whether CAF1 is part of the piRNA-containing complex. To this end, we transfected GC-2spd(ts) cells with Myc-CAF1 and mouse testicular piRNAs (test piRs), with or without Flag-MIWI. Interestingly, piRNAs can be detected in Myc-CAF1 immunoprecipitates even without exogenous Flag-MIWI, and such association was diminished upon *Miwi* knockdown (Figure 3F, lane 3 vs 6), suggesting an association mediated by endogenous MIWI in these cells. As expected, the piRNA-CAF1 association could be further enhanced by overexpressed Flag-MIWI (Figure 3F, lane 6 vs 9). On the other hand, piRNA loading onto MIWI appears independent of CAF1 as ectopically expressed Flag-MIWI efficiently coprecipitated with similar amounts of piRNAs in the presence or absence of Myc-CAF1 (Figure 3F, lane 8 vs 11). Together, these results suggest that CAF1 physically interacts with the MIWI/piRNA complex, and the resulting CAF1-containing pi-RISC acts to induce target mRNA deadenylation followed by decay.

The pi-RISC is predominantly assembled in ES

In principle, selective expression of a key pi-RISC component(s) or regulated assembly of the pi-RISC may be responsible for timing mRNA elimination in a defined

phase of spermiogenesis. To begin to explore these possibilities, we isolated spermatocytes (SC), round spermatids (RS), elongationg spermatids (ES), and elongated spermatids (Ed) from adult mouse testes by unit gravity sedimentation coupled with fluorescence-activated cell sorting (FACS) sorting as described previously [37, 41], and characterized the specificity of each isolated cell population based on their unique nuclear morphology (Supplementary information, Figure S6).

Using these carefully staged cells, we confirmed by western blot and immunostaining that both MIWI and CAF1 are readily detectable in male germ cells at all developmental stages except Ed (Figure 4A, bottom panels; Figure 4B; see also [6]). While it remains a formal pos-

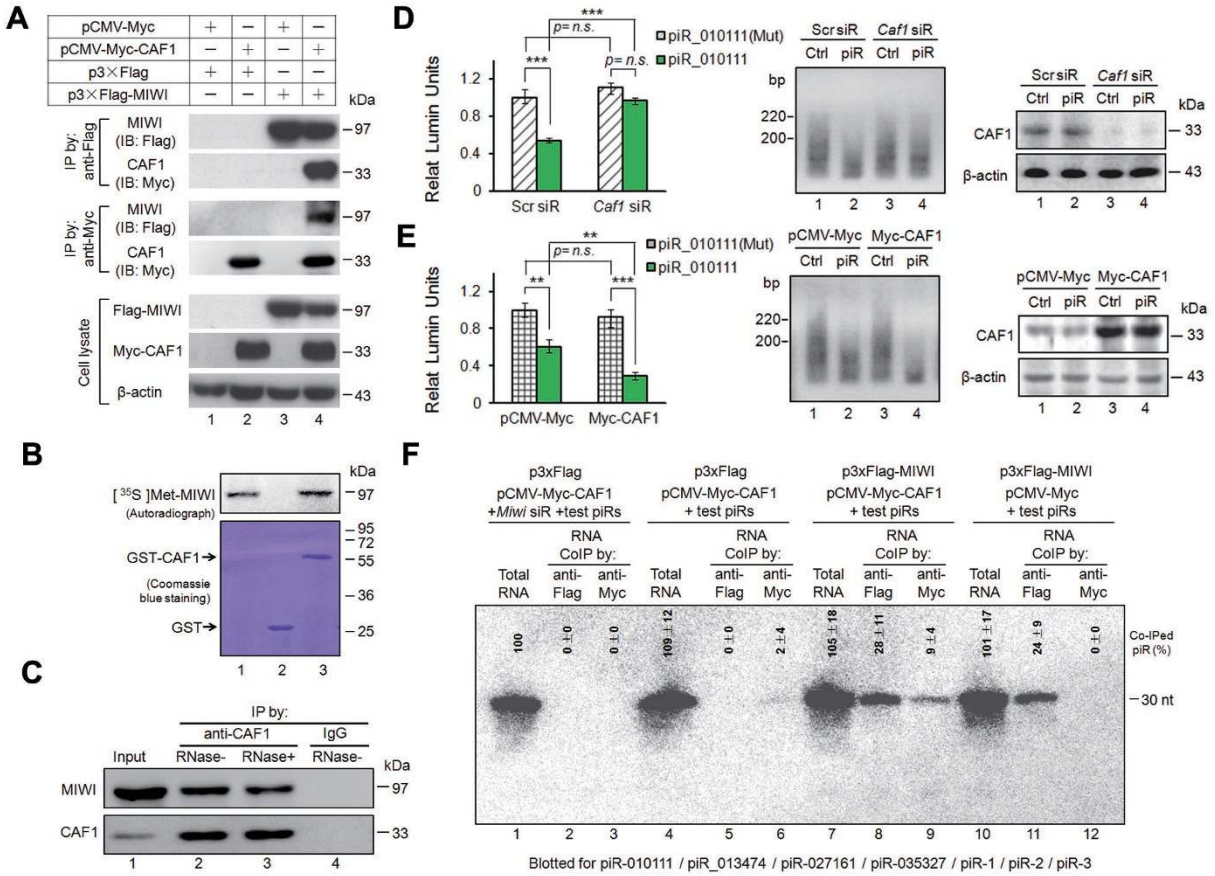

Figure 3 CAF1 is a key partner of MIWI in piRNA-induced target repression. **(A)** Co-IP assays of the interaction between Myc-CAF1 and Flag-MIWI in GC-2spd (ts) cells. Anti-Flag IP (top) and anti-Myc IP pellets (middle) were respectively immunoblotted by anti-Myc and anti-Flag antibodies. Bottom, cell lysates immunoblotted by anti-Flag or anti-Myc antibodies, with β-actin serving as a loading control. **(B)** GST pull-down assays of the interaction between CAF1 and MIWI. The GST-fused CAF1 was generated in bacteria and purified. [^{35}S]-Met-MIWI protein prepared by *in vitro* transcription/translation was incubated with GST (lane 2) or GST-CAF1 (lane 3), respectively. Input represents 10% of [^{35}S]-Met-MIWI (lane 1). Samples were analyzed by autoradiography (top) or visualized by Coomassie blue staining (bottom). **(C)** Co-IP assays of the interaction between endogenous CAF1 and MIWI in adult mouse testes. Anti-CAF1 IP pellets from RNase A untreated (lane 2) or treated testis lysate (lane 3) immunoblotted by anti-MIWI (top) and anti-CAF1 (bottom) antibodies, respectively. Immunoblot of MIWI or CAF1 in testis lysate (lane 1) or IgG IP pellet (lane 4) served as positive and negative controls, respectively. **(D** and **E)** The effect of *Caf1* knockdown **(D)** or ectopic Myc-CAF1 **(E)** on piR_010111-induced *Grk4* reporter repression in GC-2spd (ts) cells. Left, dual-luciferase reporter assays. Middle, PAT assays. Right, western blot assays of CAF1 proteins, with β-actin serving as a loading control. **(F)** RIP combined with northern blot assays of pi-RISC complex assembly in GC-2spd (ts) cells. Cells were cotransfected with the indicated expression vectors and mouse test piRs plus *Miwi* siR (lanes 1-3) or test piR (lanes 4-12). Anti-Flag RIP (lanes 2, 5, 8, and 11) and anti-Myc RIP (lanes 3, 6, 9, and 12) were blotted with the probes of piR_010111, piR_013474, piR_027161, piR_035327, piR-1, piR-2, and piR-3. Total RNAs from respective transfected cells served as positive controls (lanes 1, 4, 7, and 10). The average values ± s.d. of three separate experiments were plotted. ***P* < 0.01, ****P* < 0.001. Results shown are representative of three independent experiments.

sibility that certain male germ cell specific cofactor(s) of the MIWI complex might be developmentally regulated, we considered the possibility that regulated assembly of the pi-RISC might contribute to the activation of the mRNA elimination machinery during spermiogenesis. We thus examined whether endogenous MIWI interacts with CAF1, and if so, whether such interaction is regulated in a developmental stage-dependent fashion. Indeed, co-IP assays using the differentially-staged male germ cells revealed the interaction between endogenous MIWI and CAF1, with the strongest interaction observed in ES (Figure 4A). Double-immunostaining with anti-MIWI and anti-CAF1 coupled with confocal microscopy with Z-stacks revealed that MIWI and CAF1 were precisely colocalized only in ES, but not in SC or RS (Figure 4B). We were also able to show by RNA-IP that much more piRNAs were associated with CAF1 in ES than in SC or RS (Figure 4C). Taken together, these results suggest that the assembly of critical components of the pi-RISC (CAF1 and MIWI) is temporally and spatially regulated during male germ cell development, reaching a peak only in ES.

piRNA-mediated decay of target mRNAs occurs in ES

Based on the elucidated timing of pi-RISC assembly, we predicted that degradation of piRNA targets would occur in a similar developmental window. To test this prediction, we first determined the expression levels of five piRNA target genes (*Grk4*, *Sox6*, *Cacna1h*, *Zkscan17*, and *Cnot1*) that we had validated earlier, in each of the germ cell populations (SC, RS, ES, and Ed) by RT-qPCR and northern blot. We found that the mRNA levels of all 5 genes were dramatically reduced in ES and became hardly detectable in Ed (Figure 5A and 5B). This programmed reduction of gene expression was also evident at the protein levels as shown by western blot (Figure 5C).

As anticipated, the PAT assays showed that the poly(A) tails of these piRNA targets began to shorten in ES and became undetectable in Ed, while no such changes were observed with the nontarget GAPDH transcript (Figure 5D). We made similar observations on the other five genes (*Nploc4*, *Samd4*, *Qrich1*, *Tcf20*, and *Ap2a1*) that were initially nonresponsive to "predicted" piRNAs, but later shown to respond to their cognate piRNAs that were identified based on the mapped MIWI CLIP peaks (Supplementary information, Figure S7). These results demonstrate that deadenylation and degradation of piRNA target mRNAs occur at a late stage of spermatid development, predominantly in ES.

Both MIWI and CAF1 are required for developmental elimination of piRNA targets

To directly document the requirement for MIWI and CAF1 in repressing piRNA targets in ES, we prepared high-titer shRNA lentivirus to knock down *Miwi* or *Caf1* (Supplementary information, Figure S8A and S8B) in ES through testis transduction as we recently described [37]. One week after viral transduction, ES were isolated and transduced cells were monitored by GFP expression. We sorted ~10^6 GFP^+ cells from ~20 mice transduced with *shMiwi*:GFP, *shCaf1*:GFP or control pSilencer:GFP, respectively. RT-qPCR analysis revealed that, downregulation of all of the 10 candidate piRNA targets we had investigated earlier was prevented in *shMiwi*:GFP- or *shCaf1*:GFP-transduced ES, but not in GFP-negative or pSilencer:GFP-transduced cells (Figure 6A and Supplementary information, Figure S8C).

The MIWI- and CAF1-dependent regulation of piRNA target genes was also evident at the protein levels in *shRNA*-transduced ES. Western blot analyses showed that in *shMiwi*:GFP- or *shCaf1*:GFP-transduced ES, the protein levels of all five examined piRNA targets (GRK4, SOX6, ZKSCAN17, CACNA1H, and CNOT1) were significantly elevated with a concomitant decrease in MIWI or CAF1 levels (Figure 6B, lanes 4 and 6). In contrast, none of these genes was significantly altered in the pSilencer:GFP-transduced control (Figure 6B, lane 2) or in GFP-negative cells from *shMiwi*- or *shCaf1*-transduced mice (lanes 3 and 5). We further validated the MIWI- and CAF1-dependent reduction of GRK4 and SOX6 by immunostaining using enriched ES (Figure 6C and 6D, Supplementary information, Figure S8A and S8B). We conclude from these results that both MIWI and CAF1 are essential for piRNA target repression in ES.

Specific piRNAs are essential for MIWI-mediated mRNA elimination

To demonstrate the central role of specific piRNAs in guiding specific mRNA elimination during spermiogenesis, we selectively inhibited the function of piR_010111 and piR_013474, two most abundant piRNAs identified in isolated MIWI complexes from ES (see Supplementary information, Figure S1C). Chemically synthesized Cy3-labeled 2′-O-methyl piRNA antisense oligonucleotides and a scrambled control (Scr anti-piR) were each introduced into adult mouse testes through electroporation. One week after electroporation, ES were isolated and affected cells were monitored by Cy3 fluorescence.

We found by RT-qPCR that the level of *Grk4* mRNA (target of piR_010111) was significantly upregulated only in anti-piR_010111-containing cells, whereas the levels of *Sox6* and *Zkscan17* mRNAs (two targets of

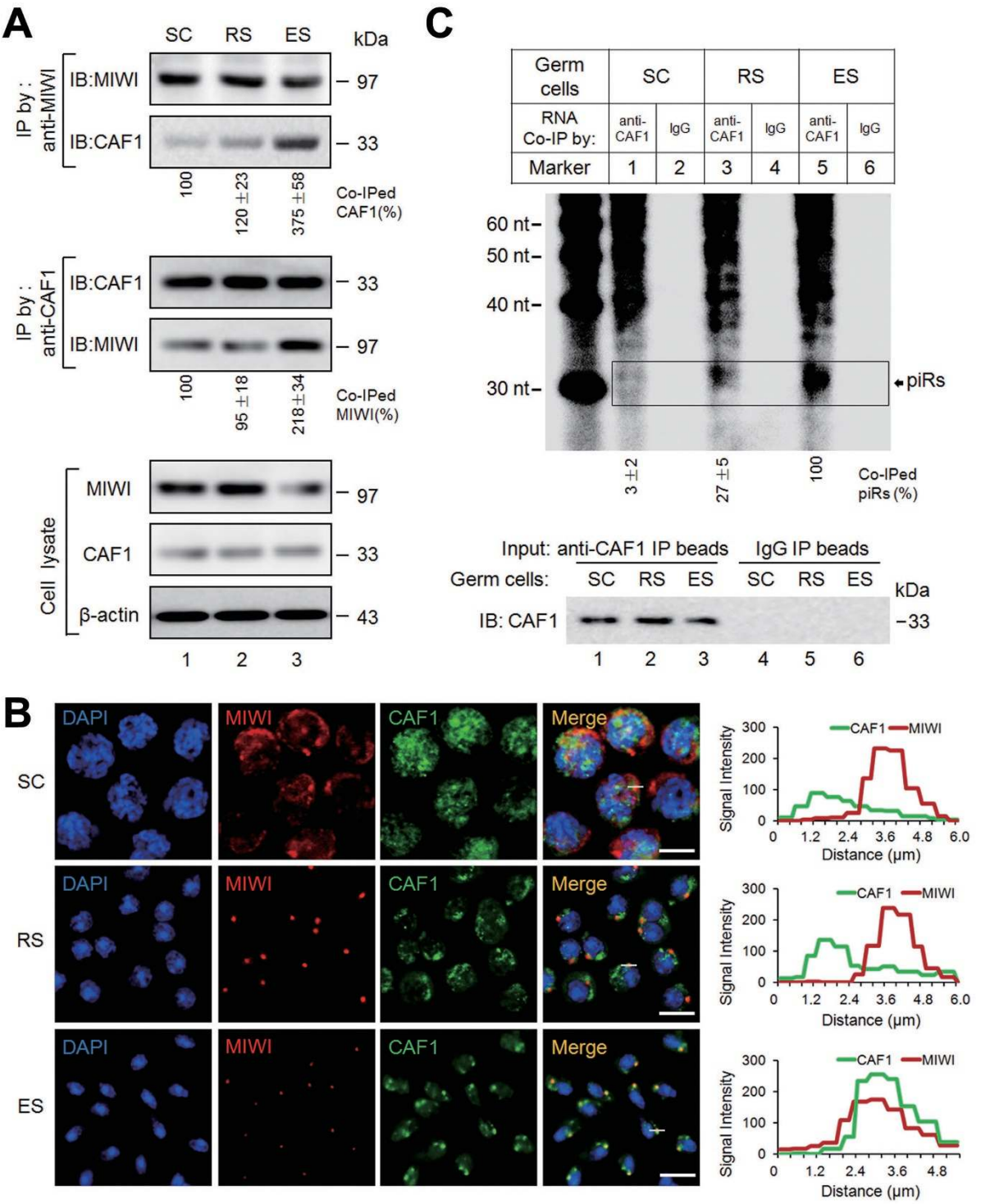

Figure 4 pi-RISC is predominantly assembled in ES. **(A)** Co-IP assays of the interaction between CAF1 and MIWI in enriched-SC (lane 1), RS (lane 2), and ES (lane 3). Anti-MIWI IP (top) and anti-CAF1 IP pellets (middle) immunoblotted by anti-CAF1 and anti-MIWI antibodies, respectively. Bottom, respective cell lysates immunoblotted by anti-MIWI or anti-CAF1 antibodies, with β-actin serving as a loading control. **(B)** Double-immunostaining of MIWI (red) and CAF1 (green) in SC (top), RS (middle), and ES (bottom). Nuclei were counterstained with DAPI (blue). Colocalization of MIWI and CAF1 was shown as yellow. Scale bar, 10 μm. Z-stacks (right) was used to project the 6.0-μm side view (*x* axis) of MIWI (red) CAF1 (green) in the lined region. **(C)** RIP assays of CAF1-associated RNAs in SC (lane 1), RS (lane 3), and ES (lane5), with IgG-IPed RNA as negative controls (lanes 2, 4, and 6), and immunoblot of IP pellets with anti-CAF1 as loading references (bottom). Results shown are representative of three independent experiments.

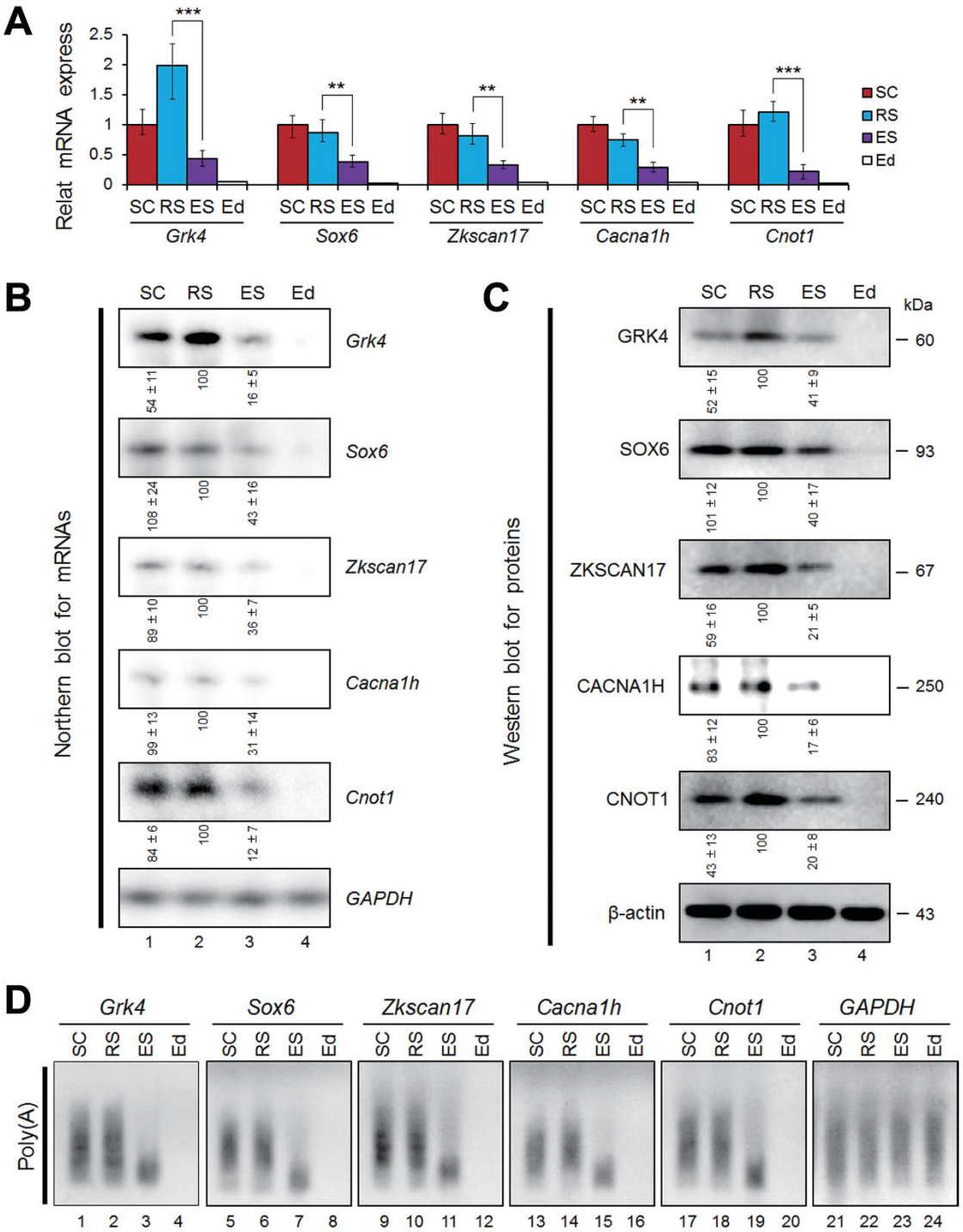

Figure 5 Decay of piRNA targets occurs in ES. **(A)** qRT-PCR assays of the mRNA levels of the five piRNA targets (*Grk4*, *Sox6*, *Zkscan17*, *Cacna1h*, and *Cnot1*) in enriched SC (red), RS (cyan), ES (purple), and Ed (white), with *GAPDH* serving as an internal control. The average values ± s.d. of three separate experiments were plotted. $^{**}P < 0.01$, $^{***}P < 0.001$. **(B** and **C)** Northern blot **(B)** or western blot analyses **(C)** of the expression of the five target genes in enriched SC (lane 1), RS (lane 2), ES (lane 3), and Ed (lane 4), with *GAPDH* **(B)** or β-actin **(C)** serving as loading controls. **(D)** PAT assays of Poly(A) tails of the five target mRNAs in enriched SC (lanes 1, 5, 9, 13, and 17), RS (lanes 2, 6, 10, 14, and 18), ES (lanes 3, 7, 11, 15, and 19), and Ed (lanes 4, 8, 12, 16, and 20), with *GAPDH* serving as a nontarget control (lanes 21-24). Results shown are representative of three independent experiments.

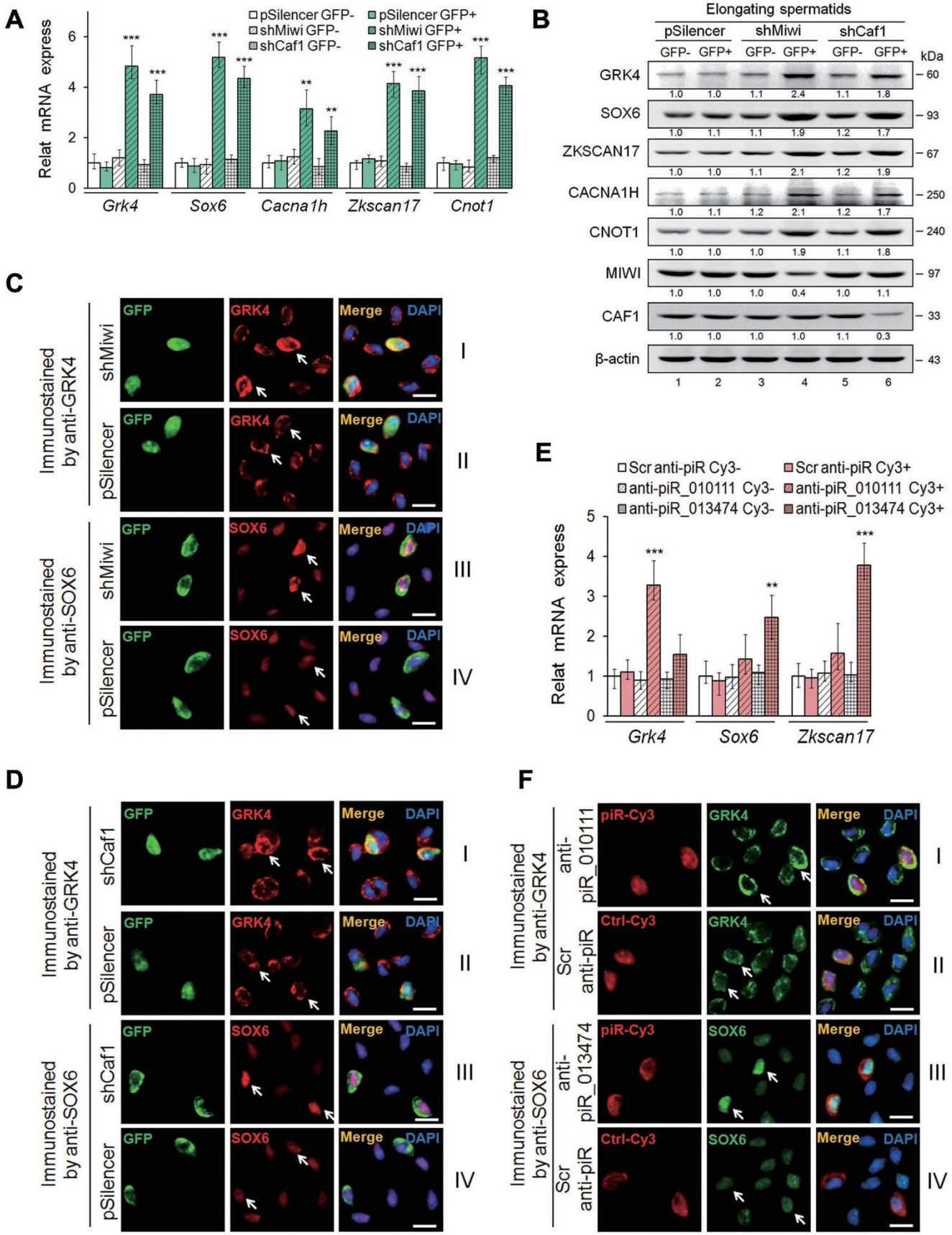
A
pSilencer GFP-
pSilencer GFP+
shMiwi GFP-
shMiwi GFP+
shCaf1 GFP-
shCaf1 GFP+
Relat mRNA express
Grk4
Sox6
Cacna1h
Zkscan17
Cnot1
B
Elongating spermatids
pSilencer
shMiwi
shCaf1
GFP-
GFP+
kDa
GRK4
SOX6
ZKSCAN17
CACNA1H
CNOT1
MIWI
CAF1
β-actin
C
Immunostained by anti-GRK4
Immunostained by anti-SOX6
shMiwi
pSilencer
GFP
GRK4
SOX6
Merge
DAPI
D
shCaf1
E
Scr anti-piR Cy3-
Scr anti-piR Cy3+
anti-piR_010111 Cy3-
anti-piR_010111 Cy3+
anti-piR_013474 Cy3-
anti-piR_013474 Cy3+
F
piR-Cy3
Ctrl-Cy3
anti-piR_010111
anti-piR_013474
Scr anti-piR

piR_013474) were increased only in anti-piR_013474-containing cells (Figure 6E). We further confirmed the expected increase of GRK4 or SOX6 protein levels by immunostaining in ES containing anti-piR_010111 or anti-piR_013474, but not in Cy3-negative or Scr anti-piR-containing cells (Figure 6F). These data demonstrate that inhibition of specific piRNAs abrogated the developmental downregulation of their cognate targets, further supporting that specific piRNAs directly mediate the repression of their targets during spermiogenesis.

The piRNA system is responsible for eliminating a large number of mRNAs in ES

We reasoned that the pi-RISC, by virtue of the enormous sequence portfolio of piRNAs, might mediate elimination of a large variety of mRNAs in late stages of spermiogenesis. Both *Miwi*-null and *Caf1*-null mice showed early spermiogenic arrest [6, 25], preventing us from determining the role of MIWI and CAF1 in ES using the existing genetic models. We therefore used *shRNA* knockdown to determine the global effect of MIWI or CAF1 on mRNA levels in ES. Using GFP^+ ES sorted from mouse testes transduced with *shMiwi*:GFP, *shCaf1*:GFP, or control pSilencer:GFP, we performed transcriptome profiling on Affymetrix mouse arrays. We identified 5 131 and 4 833 mRNAs that were dramatically upregulated (by > threefold) in *shMiwi*- and *shCaf1*-transduced cells, respectively, relative to control *shRNA*-treated cells (Figure 7A and 7B and Supplementary information, Figure S9A and Table S4), which represent ~40% of 12 917 mRNAs detectable in ES (see below). Such dramatic MIWI- or CAF1-dependent regulation of gene expression most likely occurs at the post-transcriptional level because transcription already ceases at the stage of ES [42, 43].

Strikingly, cross analysis revealed that 4 559 mRNAs (representing ~94% of *shCaf1*-upregulated mRNAs and ~89% of *shMiwi*-upregulated mRNAs) were shared between MIWI- and CAF1-regulated mRNAs (Figure 7A and 7B), strongly supporting the notion that MIWI and CAF1 act in the same pathway to mediate the degradation of a large group of mRNAs in ES. Moreover, cross analysis showed that 2 609 out of the 4 559 MIWI/CAF1-coregulated mRNAs (representing ~60% of MIWI/CAF1-coregulated mRNAs) were overlapped with MIWI-CLIPed mRNAs (Figure 7B; $P = 7.36 \times 10^{-284}$, Fisher's exact test), lending further support to the mechanism of pi-RISC-mediated mRNA elimination. The non-overlapped genes (i.e., 1,950 MIWI/CAF1-coregulated genes not detected by CLIP-seq, or 4 457 MIWI-CLIPed mRNAs not significantly upregulated upon *Miwi* or *Caf1* knockdown) likely reflect different sensitivities of the methods used (i.e., CLIP-seq vs microarrays) and specific cut-offs used in data analysis. This notion is supported by the observation based on transcriptome analysis of ES (see below) that the averaged levels of 7 382 MIWI CLIPed-mRNAs were apparently higher than those of 4 559 MIWI/CAF1-coregulated mRNAs (Supplementary information, Figure S9C), suggesting that MIWI CLIP tends to catch target genes with higher expression levels, while knockdown of *Miwi* or *Caf1* tends to detect upregulated genes that were initially expressed at lower levels.

Considering the enormous repertoire of piRNA targeting capacity, we reasoned that authentic piRNA targets in ES should be more than those detected by *Miwi* or *Caf1* knockdown. To explore this, we performed a systematic transcriptome analysis of ES by RNA-seq, which identified a total of 363 847 piRNAs and 12 917 mRNAs (Supplementary information, Table S5). We found that each mRNA on average contains ~13 piRNA target sites in their 3′UTRs. Even for GAPDH, which has been considered as a nontarget control, we detected two potential

Figure 6 The components of pi-RISC are required for piRNA target repression. **(A** and **B)** The effect of *Miwi* or *Caf1* knockdown on the expression of the five piRNA targets (*Grk4*, *Sox6*, *Zkscan17*, *Cacna1h,* and *Cnot1*) in ES. GFP^+ cells were sorted from the ES isolated from *shMiwi*:GFP-, *shCaf1*:GFP-, or control pSilencer:GFP-transduced mice. **(A)** qRT-PCR assays of their mRNA levels, with *GAPDH* serving as an internal control. The respective treatments were indicated in parentheses. **(B)** Western blot assays of their protein levels in GFP^+ cells from control pSilencer:GFP (lane 2), *shMiwi*:GFP (lane 4), or *shCaf1*:GFP (lane 6), with respective GFP^- cells (lanes 1, 3, and 5) as negative controls. β-actin served as an internal reference. **(C** and **D)** Immunostaining of GRK4 (panels I and II, red) and SOX6 proteins (panels III and IV, red) in ES transduced by *shMiwi*:GFP (**C**, panels I and III), *shCaf1*:GFP (**D**, panels I and III), or control pSilencer:GFP (**C** and **D**, panels II and IV). **(E** and **F)** The effect of inhibition of piRNA function on piRNA target expression in ES. **(E)** qRT-PCR assays of the mRNA levels of *Grk4* (piR_010111 target), and *Sox6* and *Zkscan17* (piR_013474 targets) in $Cy3^+$ ES, with *GAPDH* serving as an internal control. The respective treatments were indicated in parentheses. $Cy3^+$ cells were sorted from ES isolated from mice electroporated by 2′-O-methyl anti-piR_010111, anti-piR_013474, or scrambled anti-piR, respectively. **(F)** Immunostaining of GRK4 (panels I and II, green) and SOX6 (panels III and IV, green) in ES electroporated by 2′-O-methyl anti-piR_010111 (panel I, red), anti-piR_013474 (panel III, red), or scramble anti-piR (panels II and IV, red), respectively. The average values ± s.d. of three separate experiments were plotted. $^{**}P < 0.01$, $^{***}P < 0.001$. Scale bar, 10 μm. Results shown are representative of three independent experiments.

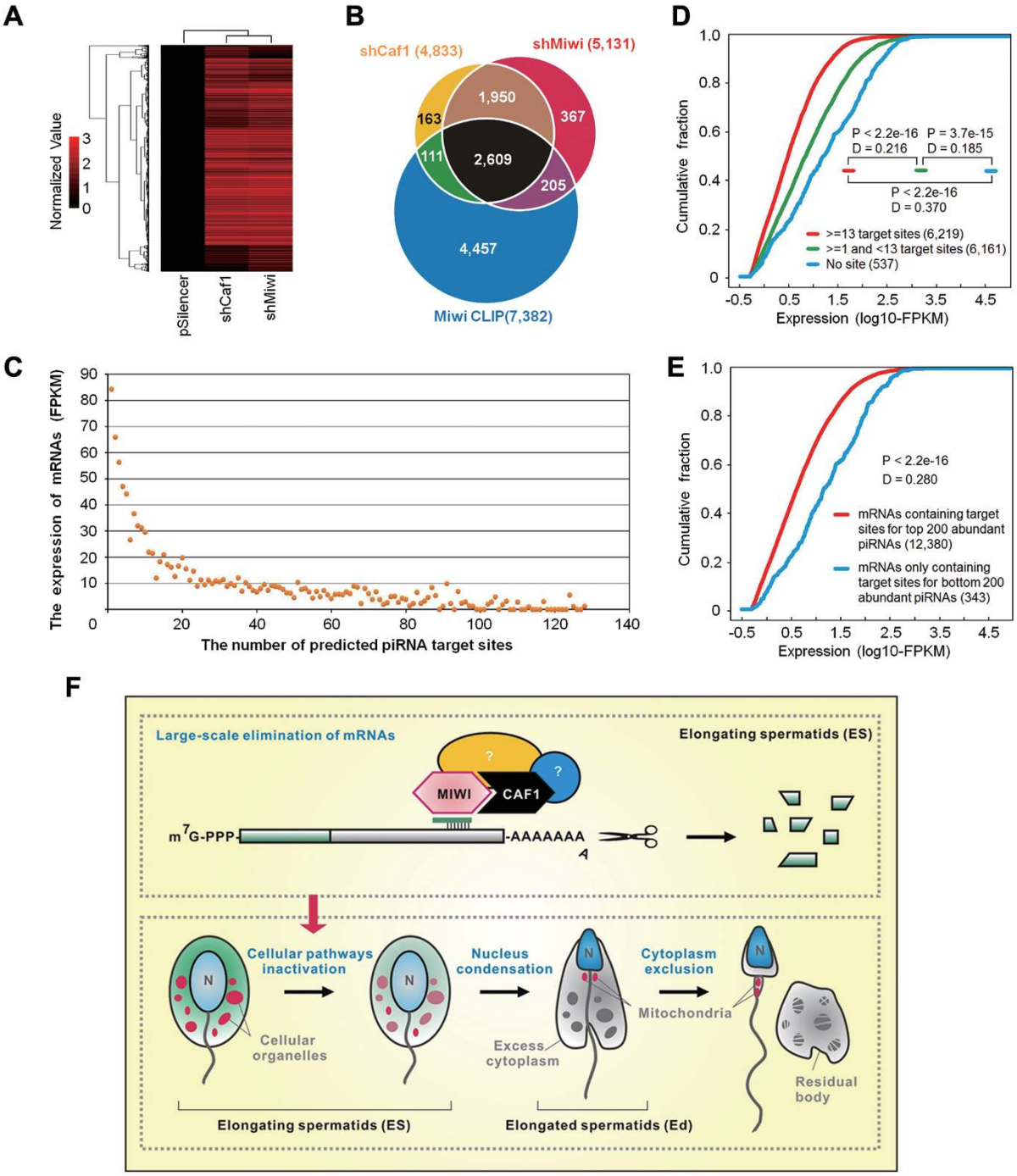

piRNA binding sites in its 3′UTR, but the two predicted piRNAs all showed very low levels of expression (Supplementary information, Table S6), thus in line with the behavior of GAPDH as a nontarget in our functional analyses (see Figure 5B and 5D) and little alteration of the transcript in response to either *Miwi* or *Caf1* knockdown (Supplementary information, Table S4).

Interestingly, our global transcriptome analysis revealed that the expression level of individual mRNAs in ES are inversely correlated with the numbers of predicted piRNA targeting sites within their 3′UTRs (Figure 7C). To further substantiate this, we divided the mRNAs detected in ES into three groups based on the numbers of predicted piRNA targeting sites: (1) 6 219 mRNAs with ≥ 13 sites, (2) 6 161 mRNAs with 1-13 sites, and (3) 537 mRNAs without an apparent site. We then com-

Figure 7 pi-RISC contributes to the mRNA eradication program during spermiogenesis. **(A)** Mouse transcriptome microarray profiling genes in ES altered by *Miwi* or *Caf1* knockdown. The total RNAs for microarray assays were from sorted GFP$^+$ ES isolated from mice transduced by pSilencer:GFP, *shMiwi*:GFP, or *shCaf1*:GFP, respectively. **(B)** Venn diagram showing the cross of genes upregulated by *Miwi* knockdown (red), *Caf1* knockdown (yellow), and MIWI-associated mRNAs characterized by CLIP-seq (blue). **(C)** The levels of mRNAs in ES inversely correlated with the numbers of potential piRNA binding sites in their 3′UTRs. *X* axis represents the number of piRNA binding sites. *Y* axis shows average expression value (FPKM) of mRNAs with same piRNA target sites. **(D** and **E)** Comparison of the cumulative abundance (log10) among three groups of mRNAs with ≥ 13 sites (red line), 1-13 sites (green line) or no apparent site (blue line) **(D)**, or between two groups of mRNAs matched to the top 200 (red line) or bottom 200 (blue line) abundant piRNAs **(E)**, as indicated in parentheses. mRNA numbers in each group were indicated and *P*- and *D*-values determined by Kolmogorov-Smirnov test (R version 2.13.0) were shown in each panel. **(F)** A model for the function of MIWI in ES, in which MIWI is assembled into a functional pi-RISC complex with guider piRNAs and deadenylase CAF1, and mediates mRNA deadenylation and decay via a miRNA-like mechanism. Such pi-RISC-triggered large-scale elimination of mRNAs in ES may facilitate nucleus condensation and cytoplasm exclusion for the completion of spermatozoa formation in mammals. Results shown are representative of three independent experiments.

pared the mRNA levels among different groups, finding that the mRNA levels in group 1 were significantly lower than group 2 (D = 0.216; $P < 2.2 \times 10^{-16}$) and group 3 (D = 0.370; $P < 2.2 \times 10^{-16}$), and those in group 2 were lower than group 3 (D = 0.185; $P = 3.7 \times 10^{-15}$) (Figure 7D, two-tailed Kolmogorov-Smirnov test). This is also evident from the much lower averaged expression of top 1 000 piRNA targets relative to that of bottom 1 000 targets (based on the numbers of potential piRNA targeting sites in the two groups of mRNAs) (Supplementary information, Figure S9D). Moreover, the levels of mRNAs that matched to the top 200 abundant piRNAs expressed in ES were significantly lower than those only matched to the bottom 200 abundant piRNAs (D = 0.280; $P < 2.2 \times 10^{-16}$) (Figure 7E). Together, these results strongly support piRNAs as key mediators in the degradation program of a large number of mRNAs in late stages of spermiogenesis.

Discussion

Unlike oocytes, which contain abundant maternal mRNAs and proteins to support early embryogenesis, sperms possess much fewer mRNAs and appear to only donate their genetic information that remains silent until zygotic activation [22, 23]. Despite such a long recognized feature of sperms, it has remained unexplored how mRNAs in haploid spermatids are purged prior to their morphological transformation into sperms. We now provide evidence that such a highly regulated program in development is largely accomplished by the piRNA system, which uses a miRNA-like mechanism to degrade their target mRNAs (Figure 7F).

An essential function of pachytene piRNAs in mRNA disposal in mammalian germ cell development

Functional characterization of pachytene piRNAs, which represent an abundant class of small RNAs in pachytene SC and haploid spermatids in mammals, has remained challenging due to the complexity of spermatogenesis and the lack of an adequate *in vitro* cell culture system for studying meiotic and post-meiotic differentiation [44]. Interestingly, a recent study shows that pachytene piRNAs are required for maintaining genome integrity in post-meiotic germline cells [45], but the molecular mechanism underlying such function of pachytene piRNAs in development has remained uncharacterized. Another recent study in *Drosophila* showed that piRNA is able to act like a miRNA to induce deadenylation and decay of a specific maternal mRNA *Nos* in early embryos [46], but it has been unclear how generally this mechanism might be utilized in development, particularly during mammalian spermatogenesis. We now demonstrate that the pachytene piRNA system in mammals, by virtue of the enormous repertoire of piRNA targeting capacity endowed by thousands of pachytene piRNA sequences in ES, is responsible for degrading a large population of mRNAs in late stages of spermiogenesis (Figure 7F), thus documenting a key function of pachytene piRNAs in spermatid development in mammals.

We showed that the function of pachytene piRNAs in inducing mRNA degradation requires a deadenylase partner besides their binding protein MIWI. Unlike *Drosophila* piRNAs utilizing deadenylase CCR4 (its mammalian homologs as CNOT6/CNOT6L) to induce the deadenylation and decay of *Nos* mRNA [46], the pachytene piRNA-mediated mRNA degradation in mouse ES depends on CAF1. CAF1 is a catalytic subunit of the previously identified CCR4-CAF1-NOT deadenylase complex involved in miRNA-mediated silencing [38-40]. However, unlike miRNA-induced gene silencing that requires CNOT1 to mediate the interactions between

CCR4-CAF1-NOT and GW182 [39, 40], we found that CNOT1 is not required for pi-RISC function. We further showed that Ago2 is also not required for piRNA-mediated target mRNA elimination. These results together suggest that piRNAs do not use the classical miRNA/siRNA machinery for the mRNA elimination program during spermiogenesis.

The function of MIWI is highly regulated during spermatogenesis

Our results suggest that MIWI, in complex with guider piRNAs and deadenylase CAF1 to assemble pi-RISC, mediates the decay of a large population of mRNAs in ES. Our finding appears to contradict with recent studies reporting that MIWI binds and translationally represses spermiogenic mRNAs in a piRNA-independent manner in mouse testes [28, 47]. Such "piRNA-independent" function might be responsible for protecting target mRNAs in SC and early RS until the next developmental phase. This possibility is consistent with our recent observation that piRNA loading to MIWI is a highly regulated process during spermatogenesis, which is inefficient in SC, but becomes highly efficient in late spermatids [37]. Importantly, our present study indicates that, in ES, MIWI is potently involved in inducing mRNA deadenylation and decay after it becomes associated with guider piRNAs and assembled into pi-RISC that contains CAF1. Our findings thus emphasize the vital piRNA-dependent function of MIWI in ES. We previously observed that MIWI is ubiquitinated in late spermatids (LS, consisting of ES and Ed) [37]. Using the carefully staged ES and Ed by unit gravity sedimentation coupled with FACS sorting, we now found that MIWI ubiquitination mainly occurs in Ed (Supplementary information, Figure S10). These results indicate that, after MIWI fulfils all of its function, the protein is subjected to APC/C-mediated ubiquitination and degradation at a late stage of spermiogenesis. Therefore, the MIWI/piRNA system appears to be precisely regulated in a highly stage-specific manner in spermatogenesis.

Our current work has further advanced the concept of regulated pi-RISC assembly by showing that MIWI and CAF1 are spatially segregated in developing germ cells. The two proteins somehow become colocalized only in ES. This may explain a dual role of MIWI in protecting or degrading mRNAs, depending on its state of piRNA loading as well as the association of CAF1. We demonstrate such a developmentally regulated process by using carefully staged cells (SC, RS, ES, and Ed) from mouse testes. In fact, we have further evidence to suggest that the function of assembled pi-RISC likely requires an additional, male germ cell-specific cofactor(s) because cotransfected MIWI and piRNAs are fully functional in promoting target mRNA degradation in GC-2spd(ts) cells, but not in HEK293T cells where CAF1 is nonetheless abundantly expressed. Identification and characterization of such a putative male germ cell-specific cofactor(s) will be an interesting objective in future studies.

The pachytene piRNA system represents an important mechanism for mRNA degradation in ES

We showed that more than half of the population of mRNAs in ES possesses ≥ 13 potential piRNA targeting sites, and the mRNA levels are inversely correlated with the number of potential target sites for piRNAs as well as the abundance of matched piRNAs. Knockdown of either *Miwi* or *Caf1* caused the up-regulation of thousands of mRNAs. These findings strongly support the idea that the pi-RISC system represents an important mechanism responsible for the elimination of mRNAs in late stages of spermiogenesis.

Considering that residual mRNAs are still detected in sperms despite that their function is under debate [23], and that there is clearly a group of mRNAs apparently not targeted by piRNAs in ES, we reason that the piRNA system is responsible for inactivating the majority of the mRNA pool, but not all mRNAs, in ES. It remains a formal possibility that the large-scale elimination of mRNAs in later stages of spermiogenesis may serve as a mechanism to dismantle multiple cellular pathways, which thus facilitates the segregation of excess cytoplasm into residual bodies. In support of this, we found no any significant gene ontology enrichment of piRNA targets (data not shown), suggesting that the pachytene piRNA system may provide an active mechanism for inactivating most cellular activities and thus allow nucleus condensation and cytoplasm exclusion for the completion of spermatozoa formation (Figure 7F).

It is also important to emphasize that not only mRNAs but also proteins are coordinately eradicated in the final phase of spermiogenesis. Our recent study showed that MIWI itself is eventually degraded in late spermatids via a ubiquitin-dependent pathway, which is essential for producing mature sperms [37]. Diminished MIWI may render its associated piRNAs vulnerable to attack by various nucleases. In any case, our current finding of pi-RISC-mediated mRNA elimination represents an important advance in our understanding of mRNA disposal in late stages of spermiogenesis, and it remains a fascinating question with respect to how removal of mRNAs and proteins contributes to the final stage of sperm formation.

Materials and Methods

Plasmids, RNA oligonucleotides, and antibodies

For reporter pRL-*Grk4* 3′UTR, the ~2.1 kb mouse *Grk4* 3′UTR was cloned downstream of the *Renilla* luciferase gene in pRL-TK (Promega). Eight nucleotides in *Grk4* 3′UTR complementary to the 5′ portion of piR_010111 were deleted for generating reporter *Grk4* 3′UTR Mut using KOD-Plus-mutagenesis kit. The wildtype and mutated 3′UTR reporters for other target candidates, including *Sox6*, *Cacna1h*, *Zkscan17*, *Cnot1*, *Nploc4*, *Samd4*, *Qrich1*, *Tcf20*, and *Ap2a1*, were similarly constructed (Figure 1C and Supplementary information, Table S2). p3×Flag-MIWI was constructed as recently described [37]. p3×Flag-HIWI and pCMV-Myc-CAF1 were constructed through insertion of the coding sequences for human *Hiwi* (NM_004764) and mouse *cnot7* (NM_011135.4) into p3×Flag-CMV-14 (Sigma) and pCMV-Myc (Clontech), respectively. HIWI mutants were constructed using p3×Flag-HIWI and KOD-Plus-mutagenesis kit. To construct GST-fused CAF1 for bacterial expression, *cnot7* cDNA (NM_011135.4) was inserted into pGEX-KG (GE Healthcare). shRNAs targeting mouse *Miwi* and *Caf1* were constructed using a lentiviral shRNA vector pSilencer-H1-LV as recently described [37], and then cotransfected with the respective target expression vector in 293T cells to test their efficacy of silencing before lentiviral packaging (Supplementary information, Figure S8A and S8B, left). All constructs were confirmed by DNA sequencing. All RNA oligonucleotides, including piRNAs and siRNAs, were synthesized by Ribobio (Guangzhou, China), and the sequences are provided in Supplementary information, Table S7.

A rabbit polyclonal anti-MIWI antibody was generated in the lab as previously reported [6]. Mouse monoclonal antibodies anti-c-Myc (M4439), anti-Flag (F3165), and anti-β-actin (A3854) were from Sigma, and anti-CAF1 (sc-101009) from Santa Cruz. Rabbit polyclonal anti-SOX6 (sc-20092), anti-ZKSCAN17 (sc-102228), anti-CACNA1H (sc-25691) were from Santa Cruz, anti-GRK4 (AP14845b) was from Abgent, anti-CNOT1 (14276-1-AP), anti-CNOT6 (17935-1-AP), and anti-GAPDH (10494-1-AP) were from Proteintech. Goat polyclonal anti-CAF1 (sc-82835) was from Santa Cruz.

Cell culture and transfection

HEK293T (293T) and GC-2spd(ts) cells were obtained from the American Type Culture Collection (ATCC) and cultured with the medium and serum as ATCC recommended. Transfection was performed using Lipofectamine 2000 (Invitrogen) according to the manufacturer's instructions. For transfection of the RNA oligonucleotides, 100~200 nM of piRNA or Scr siRNA oligonucleotides were used. For plasmid, 4 μg DNA was used in a six-well plate. All chemically synthetic piRNAs used for cell culture transfection are 2′-O-methyl modified at their 3′ ends.

RIP and CLIP assays

For RIP, ES were homogenized in Lysis Buffer (50 mM Tris-HCl (pH 7.4), 1% Triton X-100, 150 mM NaCl, 5 mM EDTA, protease inhibitor cocktail and RNase inhibitor). Cell extracts were incubated with the MIWI antibody-coupled Protein A/G beads for 4-6 h. After washing the beads with washing buffer (50 mM Tris-HCl (pH 7.4), 0.1% Triton X-100, 500 mM NaCl, 5 mM EDTA, protease inhibitor cocktail, and RNase inhibitor), total RNAs were isolated with TRIzol for deep sequencing. The CLIP was performed as recently described [33]. In brief, ES were UV irradiated (254 nm) at 400 mJ in 15-cm plate before immunoprecipitation(IP) by an anti-MIWI antibody. IPed RNA-protein complexes were digested with micrococcal nuclease, labeled with γ-[^{32}P]-ATP (PerkinElmer) by T4 PNK (Fermentas), and isolated by SDS-PAGE, in which [^{32}P]-labeled RNA-protein bands were cut for extracting RNAs for deep sequencing.

Deep sequencing, microarray, and bioinformatic analyses

MIWI RIPed and CLIPed RNAs, and transcriptome in ES were sequenced using the Illumina sequencing technology. All sequencing reads from large RNA library were mapped to the mouse reference genome (NCBI 37, mm9) using the TopHat software [48]. The genome-matching reads were used to measure gene abundance using Cufflinks software [49]. Cufflinks outputs gene transcript abundance as fragments per kilobase of exon per million mapped reads (FPKM). For RIP-seq, MIWI-RIPed mRNAs were defined as anti-MIWI IP-Seq FPKM/negative control FPKM ≥ 1.5 and false discovery rate (FDR) < 0.05. Reads with same 5′ sequences were classified into one type of piRNAs and piRNAs with ≥ 1 000 reads were used for prediction of piRNA:mRNA interactions. For CLIP-seq, reads were processed as recently described [33, 50, 51]. In brief, reads with length from 25-33 nt and > 33 nt at a cut-off of 5 were respectively selected as candidate piRNAs and target peaks. The target peaks were further filtered to remove those overlapped with piRNA clusters, and then extended by an additional 30 nt in both 5′- and 3′-directions as inputs for miRanda program [30]. For transcriptome-seq, mRNA abundance also were measured using Cufflinks software [49]. The top 200 abundant piRNAs were used for prediction of piRNA targets from the 3′UTR of mRNAs using miRanda software [30] with options: -strict -quiet. Two-sided Kolmogorov-Smirnov statistics (in the R package, http://cran.r-project.org/) was used to determine the significance of the shift in pairwise comparison. Annotation: all unique reads without adapters in each small RNA library were mapped to the mouse genomes (UCSC mm9) using Bowtie (version 0.12.7) [52] with options: -f -a --best --strata -v 2 -m 100, and reads mapping to > 100 region or reads with > 2 mismatches were discarded. The genome-matching reads were annotated by intersecting them with the annotated genomic elements coordinates. And annotation categories were used by the priority: (i) miRNA, (ii) ncRNA, (iii) mRNA, (iv) Intron, and (v) repetitive sequences.

For transcriptome genechip assays, total RNAs from biological triplicates of pSilencer:GFP-, *shMiwi*:GFP-, or *shCaf1*:GFP-ES were extracted using TRIzol (Invitrogen). Gene expression analyses using Affymetrix mouse GeneChip 430 2.0 arrays were performed in Shanghai Biotechnology Corporation. The data were analyzed using Genespring GX software (Agilent Technologies).

Luciferase reporter assays

Luciferase reporter assays were carried out as we described previously [53]. In brief, each 3′UTR-Renilla luciferase reporter construct was cotransfected into GC-2spd(ts) cells in 24-well plates with firefly luciferase plasmid pGL3 (as an internal control) and RNA oligonucleotides or vectors as indicated in Figures 1-3, Supplementary information, Figures S3-S5. piRNA negative controls were designed as the mutated forms of their cognate piRNAs (designated as piR_xxx(Mut)) with a change of 7-nt sequences at 5′-end for disrupting the base pairing between piRNAs and target mRNAs, and the sequences are provided in Supplementary infor-

mation, Table S7. All the reporter activity assays were performed 24 h after transfection.

PAT assays

PAT assays were performed as described previously [54, 55] with specific primers (the sequences listed in Supplementary information, Table S7). In brief, total RNAs extracted from cells were incubated with poly[dT]$_{12-18}$, oligo[dT]-anchor, and T4 DNA ligase before reverse transcription reaction for generating PAT cDNA. The polyadenylation state of mRNAs was analyzed by PCR using a message-specific primer, oligo(dT)-anchor primer, and PAT cDNA.

Slicer assay

The assays were carried out as described previously [13]. In brief, a synthetic 40-nt RNA bearing complementary to piR-1 was [^{32}P]-labeled and used as the target (see Figure 2C). piR-1 loaded HIWI or its slicer activity-deficient ADH [13] and piRNA loading-deficient Y345/346A mutants [37] were immunopurified from Flag-HIWI or its mutant vectors and piR-1 cotransfected GC-2-spd(ts) cells and mixed with a 5′-[^{32}P]-labeled RNA target. The apo-HIWI or its mutants, which were similarly purified with Flag antibody from Flag-HIWI-transfected cells, were used as negative controls in the assays. After the *in vitro* reaction, RNAs were extracted and resolved on a 15%, 7 M urea polyacrylamide gel, followed by autoradiography.

Biochemical and cell biology assays

IP, immunoblotting, GST pulldown, and northern blot assays were carried out as we described recently [37]. For Immunostaining, the isolated spermatogenic cells were fixed with 4% paraformaldehyde, permeabilized with 0.5% Triton X-100 in PBS, and incubated with respective primary antibodies and Alexa Fluor 488 or Cy3-conjugated secondary antibodies. Nuclei were counterstained with DAPI (Vector Laboratories). Laser confocal scanning images were captured using a Leica TCS SP5 inverted spectral confocal microscopy with projection of 6.0-μm Z-stacks.

Isolation of mouse spermatogenic cells

Isolation of mouse SC, RS, and late spermatids (consisting of ES and Ed) was performed using unit gravity velocity sedimentation as we recently described [37]. The separation of ES from Ed were through FACS procedure modified from methods described previously [41]. In brief, the elongating/Ed suspensions were incubated in a staining solution (3 μg/ml DNase I (Fermentas), 5 μg/ml Hoechst 33342 (Acros Organics), 2 μg/ml propidium iodine (Sigma)) for 30 min at 33 °C, then filtered through two stacked GBSS wetted 40 μm strainers (Fisher) to remove small clumps and debris for FACS. The two types of spermatids showed distinguished forward scatter parameter (FSC), which allows the separation of them in two subpopulations. The FSC^{high} and FSC^{low} populations represent ES and Ed, respectively. The isolated spermatogenic cells were all confirmed by their distinct nuclear morphology (DAPI staining of nuclei; see Supplementary information, Figure S6).

Lentivirus transduction and piRNA electroporation of mouse testis

Lentivirus packaging and testis transduction were performed as we recently described [37]. RNA electroporation were carried out as previously described [56]. In brief, Cy3-labeled piRNAs were injected into seminiferous tubules through efferent duct by a sharp glass capillary with a tip diameter of 50 μm, following with electric pulses by an Electrosquare Porator T830 electric pulse generator (BTX, USA). The testes were harvested one week post-electroporation of RNA oligonucleotides. Due to low efficiency of electroporation, we could only sort ~10^3 Cy3$^+$ cells from ES that were isolated from ~20 electroporation mice.

Animal work

ICR and C57BL/6J mice were used in this study. All experimental animal procedures were approved by the Institutional Animal Care and Research Advisory Committee at IBCB, SIBS, CAS.

Statistical analysis

The results are presented as the mean ± standard error (SD) of the mean. A Student's *t*-test was used to compare the differences between treated groups relative to their paired controls. *P*-values are indicated in the text and figures above the two groups compared. Differences were considered significant when $P < 0.05$.

Acknowledgments

We thank Drs Narry Kim (Seoul National University, Korea) and Fátima Gebauer (Centre for Genomic Regulation, Spain) for suggestions and critical comments on the manuscript; Drs Chen Chu, Junhao Li, and Xianghua Piao for experimental and bioinformatic assistance. This work was supported by grants from the Ministry of Science and Technology of China (2011CB811303, 2014CB964802, 2014CB943103, 2012CB910803), the National Natural Science Foundation of China (31325008, 91219306, 31270840, 31170754, 31300656), and Science and Technology Commission of Shanghai Municipality (13ZR1464300).

References

1 Aravin A, Gaidatzis D, Pfeffer S, *et al.* A novel class of small RNAs bind to MILI protein in mouse testes. *Nature* 2006; **442**:203-207.
2 Girard A, Sachidanandam R, Hannon GJ, Carmell MA. A germline-specific class of small RNAs binds mammalian Piwi proteins. *Nature* 2006; **442**:199-202.
3 Grivna ST, Beyret E, Wang Z, Lin H. A novel class of small RNAs in mouse spermatogenic cells. *Genes Dev* 2006; **20**:1709-1714.
4 Lau NC, Seto AG, Kim J, *et al.* Characterization of the piRNA complex from rat testes. *Science* 2006; **313**:363-367.
5 Cox DN, Chao A, Baker J, Chang L, Qiao D, Lin H. A novel class of evolutionarily conserved genes defined by piwi are essential for stem cell self-renewal. *Genes Dev* 1998; **12**:3715-3727.
6 Deng W, Lin H. miwi, a murine homolog of piwi, encodes a cytoplasmic protein essential for spermatogenesis. *Dev Cell* 2002; **2**:819-830.
7 Klattenhoff C, Bratu DP, McGinnis-Schultz N, Koppetsch BS, Cook HA, Theurkauf WE. *Drosophila* rasiRNA pathway mutations disrupt embryonic axis specification through activation of an ATR/Chk2 DNA damage response. *Dev Cell* 2007;

12:45-55.
8 Carmell MA, Girard A, van de Kant HJ, *et al.* MIWI2 is essential for spermatogenesis and repression of transposons in the mouse male germline. *Dev Cell* 2007; **12**:503-514.
9 Houwing S, Kamminga LM, Berezikov E, *et al.* A role for Piwi and piRNAs in germ cell maintenance and transposon silencing in Zebrafish. *Cell* 2007; **129**:69-82.
10 Gunawardane LS, Saito K, Nishida KM, *et al.* A slicer-mediated mechanism for repeat-associated siRNA 5′ end formation in Drosophila. *Science* 2007; **315**:1587-1590.
11 Aravin AA, Sachidanandam R, Bourc'his D, *et al.* A piRNA pathway primed by individual transposons is linked to *de novo* DNA methylation in mice. *Mol Cell* 2008; **31**:785-799.
12 De Fazio S, Bartonicek N, Di Giacomo M, *et al.* The endonuclease activity of Mili fuels piRNA amplification that silences LINE1 elements. *Nature* 2011; **480**:259-263.
13 Reuter M, Berninger P, Chuma S, *et al.* Miwi catalysis is required for piRNA amplification-independent LINE1 transposon silencing. *Nature* 2011; **480**:264-267.
14 Siomi MC, Sato K, Pezic D, Aravin AA. PIWI-interacting small RNAs: the vanguard of genome defence. *Nat Rev Mol Cell Biol* 2011; **12**:246-258.
15 Thomson T, Lin H. The biogenesis and function of PIWI proteins and piRNAs: progress and prospect. *Annu Rev Cell Dev Biol* 2009; **25**:355-376.
16 Luteijn MJ, Ketting RF. PIWI-interacting RNAs: from generation to transgenerational epigenetics. *Nat Rev Genet* 2013; **14**:523-534.
17 Meikar O, Da Ros M, Korhonen H, Kotaja N. Chromatoid body and small RNAs in male germ cells. *Reproduction* 2011; **142**:195-209.
18 Kuramochi-Miyagawa S, Watanabe T, Gotoh K, *et al.* DNA methylation of retrotransposon genes is regulated by Piwi family members MILI and MIWI2 in murine fetal testes. *Genes Dev* 2008; **22**:908-917.
19 Watanabe T, Tomizawa S, Mitsuya K, *et al.* Role for piRNAs and noncoding RNA in *de novo* DNA methylation of the imprinted mouse Rasgrf1 locus. *Science* 2011; **332**:848-852.
20 Yan W. Male infertility caused by spermiogenic defects: lessons from gene knockouts. *Mol Cell Endocrinol* 2009; **306**:24-32.
21 Hess RA, Renato de Franca L. Spermatogenesis and cycle of the seminiferous epithelium. *Adv Exp Med Biol* 2008; **636**:1-15.
22 Stitzel ML, Seydoux G. Regulation of the oocyte-to-zygote transition. *Science* 2007; **316**:407-408.
23 Lalancette C, Miller D, Li Y, Krawetz SA. Paternal contributions: new functional insights for spermatozoal RNA. *J Cell Biochem* 2008; **104**:1570-1579.
24 Lau NC, Kolkman A, van Schaik FM, *et al.* Human Ccr4-Not complexes contain variable deadenylase subunits. *Biochem J* 2009; **422**:443-453.
25 Berthet C, Morera AM, Asensio MJ, *et al.* CCR4-associated factor CAF1 is an essential factor for spermatogenesis. *Mol Cell Biol* 2004; **24**:5808-5820.
26 Sassone-Corsi P. Unique chromatin remodeling and transcriptional regulation in spermatogenesis. *Science* 2002; **296**:2176-2178.
27 Dadoune JP, Siffroi JP, Alfonsi MF. Transcription in haploid male germ cells. *Int Rev Cytol* 2004; **237**:1-56.
28 Vourekas A, Zheng Q, Alexiou P, *et al.* Mili and Miwi target RNA repertoire reveals piRNA biogenesis and function of Miwi in spermiogenesis. *Nat Struct Mol Biol* 2012; **19**:773-781.
29 Beyret E, Liu N, Lin H. piRNA biogenesis during adult spermatogenesis in mice is independent of the Ping-Pong mechanism. *Cell Res* 2012; **22**:1429-1439.
30 John B, Enright AJ, Aravin A, Tuschl T, Sander C, Marks DS. Human MicroRNA targets. *PLoS Biol* 2004; **2**:e363.
31 Hofmann MC, Abramian D, Millan JL. A haploid and a diploid cell coexist in an *in vitro* immortalized spermatogenic cell line. *Dev Genet* 1995; **16**:119-127.
32 Wu L, Fan J, Belasco JG. MicroRNAs direct rapid deadenylation of mRNA. *Proc Natl Acad Sci USA* 2006; **103**:4034-4039.
33 Xue Y, Ouyang K, Huang J, *et al.* Direct conversion of fibroblasts to neurons by reprogramming PTB-regulated microRNA circuits. *Cell* 2013; **152**:82-96.
34 Lee HC, Gu W, Shirayama M, Youngman E, Conte D Jr, Mello CC. *C. elegans* piRNAs mediate the genome-wide surveillance of germline transcripts. *Cell* 2012; **150**:78-87.
35 Bagijn MP, Goldstein LD, Sapetschnig A, *et al*. Function, targets, and evolution of *Caenorhabditis elegans* piRNAs. *Science* 2012; **337**:574-578.
36 Meister G. Argonaute proteins: functional insights and emerging roles. *Nat Rev Genet* 2013; **14**:447-459.
37 Zhao S, Gou LT, Zhang M, *et al*. piRNA-triggered MIWI ubiquitination and removal by APC/C in late spermatogenesis. *Dev Cell* 2013; **24**:13-25.
38 Piao X, Zhang X, Wu L, Belasco JG. CCR4-NOT deadenylates mRNA associated with RNA-induced silencing complexes in human cells. *Mol Cell Biol* 2010; **30**:1486-1494.
39 Behm-Ansmant I, Rehwinkel J, Doerks T, Stark A, Bork P, Izaurralde E. mRNA degradation by miRNAs and GW182 requires both CCR4:NOT deadenylase and DCP1:DCP2 decapping complexes. *Genes Dev* 2006; **20**:1885-1898.
40 Braun JE, Huntzinger E, Fauser M, Izaurralde E. GW182 proteins directly recruit cytoplasmic deadenylase complexes to miRNA targets. *Mol Cell* 2011; **44**:120-133.
41 Bastos H, Lassalle B, Chicheportiche A, *et al*. Flow cytometric characterization of viable meiotic and postmeiotic cells by Hoechst 33342 in mouse spermatogenesis. *Cytometry A* 2005; **65**:40-49.
42 Geremia R, Boitani C, Conti M, Monesi V. RNA synthesis in spermatocytes and spermatids and preservation of meiotic RNA during spermiogenesis in the mouse. *Cell Differ* 1977; **5**:343-355.
43 Steger K. Haploid spermatids exhibit translationally repressed mRNAs. *Anat Embryol (Berl)* 2001; **203**:323-334.
44 Yadav RP, Kotaja N. Small RNAs in spermatogenesis. *Mol Cell Endocrinol* 2013; **382**:498-508.
45 Zheng K, Wang PJ. Blockade of pachytene piRNA biogenesis reveals a novel requirement for maintaining post-meiotic germline genome integrity. *PLoS Genet* 2012; **8**:e1003038.
46 Rouget C, Papin C, Boureux A, *et al.* Maternal mRNA deadenylation and decay by the piRNA pathway in the early Drosophila embryo. *Nature* 2010; **467**:1128-1132.
47 Nishibu T, Hayashida Y, Tani S, *et al.* Identification of MIWI-

associated Poly(A) RNAs by immunoprecipitation with an anti-MIWI monoclonal antibody. *Biosci Trends* 2012; **6**:248-261.
48 Trapnell C, Pachter L, Salzberg SL. TopHat: discovering splice junctions with RNA-Seq. *Bioinformatics* 2009; **25:**1105-1111.
49 Trapnell C, Roberts A, Goff L, *et al*. Differential gene and transcript expression analysis of RNA-seq experiments with TopHat and Cufflinks. *Nat Protoc* 2012; **7**:562-578.
50 Fejes AP, Robertson G, Bilenky M, Varhol R, Bainbridge M, Jones SJ. FindPeaks 3.1: a tool for identifying areas of enrichment from massively parallel short-read sequencing technology. *Bioinformatics* 2008; **24**:1729-1730.
51 Karginov FV, Hannon GJ. Remodeling of Ago2-mRNA interactions upon cellular stress reflects miRNA complementarity and correlates with altered translation rates. *Genes Dev* 2013; **27**:1624-1632.
52 Langmead B, Trapnell C, Pop M, Salzberg SL. Ultrafast and memory-efficient alignment of short DNA sequences to the human genome. *Genome Biol* 2009; **10**:R25.
53 Jiang S, Zhang HW, Lu MH, *et al.* MicroRNA-155 functions as an OncomiR in breast cancer by targeting the suppressor of cytokine signaling 1 gene. *Cancer Res* 2010; **70**:3119-3127.
54 Salles FJ, Strickland S. Analysis of poly(A) tail lengths by PCR: the PAT assay. *Methods Mol Biol* 1999; **118**:441-448.
55 Juge F, Zaessinger S, Temme C, Wahle E, Simonelig M. Control of poly(A) polymerase level is essential to cytoplasmic polyadenylation and early development in Drosophila. *EMBO J* 2002; **21**:6603-6613.
56 Shoji M, Chuma S, Yoshida K, Morita T, Nakatsuji N. RNA interference during spermatogenesis in mice. *Dev Biol* 2005; **282**:524-534.

(**Supplementary information** is linked to the online version of the paper on the *Cell Research* website.)